

BSc Fabian Öhlinger

Digital extraction of discontinuity set orientation  
for the assessment of rock slope stability

**MASTERARBEIT**

zur Erlangung des akademischen Grades

Master of Science

Masterstudium Erdwissenschaften

eingereicht an der

Technischen Universität Graz

Betreuer

Ao.Univ.-Prof. Dr. Qian Liu

Institut für Angewandte Geowissenschaften

Graz, Oktober 2019

## **EIDESSTATTLICHE ERKLÄRUNG**

### ***AFFIDAVIT***

Ich erkläre an Eides statt, dass ich die vorliegende Arbeit selbstständig verfasst, andere als die angegebenen Quellen/Hilfsmittel nicht benutzt, und die den benutzten Quellen wörtlich und inhaltlich entnommenen Stellen als solche kenntlich gemacht habe. Das in TUGRAZonline hochgeladene Textdokument ist mit der vorliegenden Masterarbeit identisch.

*I declare that I have authored this thesis independently, that I have not used other than the declared sources/resources, and that I have explicitly indicated all material which has been quoted either literally or by content from the sources used. The text document uploaded to TUGRAZonline is identical to the present master's thesis.*

---

Datum / Date

---

Unterschrift / Signature

## Kurzfassung

Das Konzept dieser Arbeit ist die semi-automatische Bestimmung von Trennflächenscharen und deren Orientierungen durch das Bearbeiten von 3D Punktwolken.

Für diesen Zweck wird eine semi-automatische Methode in MATLAB implementiert, welche weitestgehend ohne menschliche Unterstützung funktioniert. Eine überwachte Methode, bei der eine verantwortliche Person die Daten bearbeitet, wird als Vergleich durchgeführt. Die Bearbeitung erfolgt dabei mit der Freeware CloudCompare und den kommerziellen Programmen RiSCAN PRO, sowie der Rocscience Software Dips 7.0.

Drei Datensätze, welche in Kaili, China aufgenommen wurden, werden untersucht und die räumliche Veränderung der Orientierungen der Trennflächenscharen bestimmt. Weiters wird eine kinematische Analyse durchgeführt, welche es erlaubt Aussagen bezüglich der potentiellen Gebirgsstabilität zu treffen.

Die überwachte Methode erweist sich als robust, aber zeitaufwändig für die durchführende Person. Dazu unterliegt sie einer Beeinflussung durch den Bearbeiter. Die semi-automatische Methode ist Großteils automatisiert, zu hohem Maße reproduzierbar und überwiegend frei von menschlichem Einfluss. Qualitativ liefert die semi-automatische Methode gute Ergebnisse für Scharen, welche als deutliche Flächen in der Öffnungsfläche auftreten. Verzerrte Orientierungen oder sogar das vollständige Fehlen von Scharen kann auftreten, wenn Trennflächen hauptsächlich durch Spuren in der Öffnungsfläche vertreten sind. Daher müssen Ergebnisse der semi-automatischen Methode überprüft werden, bevor Gewissheit über ihre Genauigkeit erreicht ist.

In Kaili wurden fünf subvertikale Kluft Scharen, welche ihre Orientierung über alle drei Lokalitäten kaum verändern und eine Schichtung, welche in allen Fällen einen geringen Einfallswinkel jedoch unterschiedliche Einfallsrichtungen aufweist, bestimmt. Die kinematische Analyse zeigt, dass keilförmiges Versagen der Hauptversagenstyp ist. Da in dieser Arbeit lediglich die geometrische Disposition für Versagen untersucht wird, müssen weitere Trennflächeneigenschaften wie Verwitterung, Durchgängigkeit, Konnektivität und Rauigkeit lokal bestimmt werden um die Stabilität genauer zu bewerten.

## Abstract

The concept of this thesis is the semi-automatic extraction of information regarding the orientation of discontinuities in a rock mass, by processing 3D point cloud data.

For this purpose, a semi-automatic methodology, which works to the greatest extent without human assistance, is implemented in MATLAB. Further a supervised methodology, where a person in charge edits the data, is executed for comparison. It is performed with the freeware CloudCompare and the commercial software RiSCAN PRO as well as the Rocscience software Dips 7.0.

Three data sets, detected in Kaili, China are investigated and the spatial change in discontinuity set orientations is determined. Further a kinematic analysis allows a statement on the potential stability of the rock slope.

The supervised methodology proves robust but time consuming for the geologist in charge and susceptible to human bias. The semi-automatic methodology is mostly automated, highly reproducible and not influenced by human bias. It delivers qualitatively comparable results to the supervised methodology for discontinuity set orientations, which are represented by distinct planes in the face. Biased orientations or even the complete absence of sets in the results are possible if discontinuity sets are mainly represented in the face by traces. For this reason, the semi-automatic methodology must be verified by a geologist, before certainty on the results' accuracy is achieved.

Five sub vertical fracture sets, which maintain their orientation over the three locations and a bedding plane, which slightly dips in changing directions, are detected. The kinematic analysis indicates wedge sliding as the primary failure mode in the area of Kaili. As the geometric disposition is investigated in this thesis, further discontinuity parameters like weathering, persistence, connectivity and roughness must be determined locally, to assess the slope stability.

# Contents

1. Introduction .....	2
2. Development in discontinuity orientation extraction .....	3
2.1. Traditional techniques .....	3
2.2. Modern techniques .....	3
3. Data .....	6
3.1. Field of work .....	6
3.2. Data size and resolution .....	9
4. Aim of the work .....	11
5. Discontinuity set orientations .....	13
5.1. Methodology .....	13
5.1.1. Supervised methodology .....	13
5.1.1.1. Computation of normal vectors .....	13
5.1.1.2. Segmentation of the point cloud .....	16
5.1.1.3. Plane modelling .....	17
5.1.1.4. Clustering .....	17
5.1.2. Semi-automatic methodology .....	18
5.1.2.1. Plane growth .....	18
5.1.2.2. Kernel Density Estimation .....	23
5.1.2.3. Spherical k-means clustering .....	26
5.2. Results .....	30
5.2.1. Supervised methodology .....	30
5.2.1.1. Long Chang .....	30
5.2.1.2. Xiang Qi Jiang Kou .....	33
5.2.1.3. Lao Hu Po coalmine .....	35
5.2.2. Semi-automatic methodology .....	37
5.2.2.1. Long Chang .....	37
5.2.2.2. Xiang Qi Jiang Kou .....	40
5.2.2.3. Lao Hu Po coalmine .....	43
5.3. Comparison of the methodologies .....	46
6. Stability analysis .....	55
6.1. Failure Modes .....	55
6.1.1. Planar sliding .....	56
6.1.2. Wedge sliding .....	56
6.1.3. Toppling .....	56
6.2. Methodology .....	57
6.3. Results .....	58
6.3.1. Supervised methodology .....	58
6.3.2. Semi-automatic methodology .....	62
7. Conclusion .....	67

# 1. Introduction

With remote sensing methods, such as laserscanning or photogrammetry, the morphology of an area can be recorded with high resolution. The result are large digital lists of points' 3D coordinates, called point clouds, which represent the surface. The objective of this thesis is the extraction of discontinuity orientation in rock slopes by using terrestrial laserscan (TLS) data. The basic idea is that the rock face consists of discontinuities, as these planes of weakness are exposed when rock detaches from the rock mass. Consequently, measuring the orientations observed in a rock face implies measuring discontinuity orientations. A semi-automatic approach, where planes are computed and measured automatically is performed and compared to a supervised approach, where the planes for measurements are manually modelled through the point cloud. The role of discontinuities, such as bedding or fracturing, is major when it comes to rock slope stability. Parallel to discontinuity planes shear and tensile strength are reduced and permeability is increased. Discontinuities create an anisotropic, non-continuous rock, which behaves directional. The most important discontinuity properties are orientation, spacing, persistence and roughness, however orientation has been ascribed the primary role. Consequently, an accurate and precise determination of the discontinuity orientations is the key aspect for a thorough stability analysis [1].

*"Since joint planes introduce such strongly directional weaknesses, the most important joint attribute can be considered to be orientation."* (Goodman 1989)

In most cases systematic discontinuity sets, thus discontinuities which form subparallel to each other, allow the extrapolation of measured orientations to a certain extent [1]. It is geologically reasonable that similar stress conditions have acted in an area and created similar discontinuities. In this thesis data from three laser scans in the region of Kaili (China) is processed and the resulting orientations are compared, to asses if this extrapolation is possible, or if there is a significant spatial change in discontinuity orientations. Another objective is the continuation of processing the obtained orientation data for the purpose of a kinematic stability analysis of the rock slope. This analysis investigates the geometry of the discontinuities with respect to the face orientation. A simple extension is made by including the friction angle to the considerations. The three failure modes planar sliding, wedge sliding and toppling are analysed.

## 2. Development in discontinuity orientation extraction

### 2.1. Traditional techniques

Discontinuity information is often obtained by conventional fieldwork, for instance scanline or window mapping surveys. The basic idea behind scanline mapping is to define a line at an outcrop. Along this line every discontinuity is recorded in terms of orientation, persistence, spacing, roughness and further parameters. In window mapping every discontinuity within a defined area is recorded [2]. This fieldwork is time consuming, therefore expensive, cannot be carried out in inaccessible or hazardous areas and is affected by human bias. Often the results are subjective and not reproducible [3].

### 2.2. Modern techniques

Remote surveying techniques like photogrammetry or terrestrial laserscanning allow the fast and large-scale collection of data. These techniques are ahead of traditional methods concerning data quality and quantity. They have the capability of recording up to hundreds of thousands of points in a short time, which contain the morphologic information of huge areas. The advanced processing power allows the analysis of this large data volume, to gain the valuable discontinuity information from the raw 3D point cloud, obtained by the laserscan. To extract this information from the point cloud, however, there is the necessity of proper data editing. In recent decades this topic has been subject to various studies.

Interactive computer-based methods allow to pick planes manually and receive a measurement from the software similar to traditional methods, where a field geologist measures individual discontinuity orientations with a compass. Interactive methods are supervised by a judging geologist, who maps plane by plane. This approach has been implemented in commercial software such as PolyWorks and ShapeMetrix 3D [4]. In this thesis a supervised methodology, where the individual planes are selected and measured, using the software RiSCAN PRO, is executed (section 4.1.1).

The semi-automatic approach has been of interest for research in recent years. The aim is to automatically derive orientation information from the data without, or only little, human assistance [5]. 3D surface reconstruction is an automatic method to establish a realistic model of mathematically described planar elements (triangles or facets) through the points of the point cloud. Slob et al. (2005) implemented this method by creating a mesh of triangles from

the point cloud and measuring each triangle orientation [6]. The software PlaneDetect [7] and Split-FX [6] are commercial programs based on this method. A different automatic approach that received a lot of attention is the direct point cloud segmentation. It classifies each point of the point cloud dependent on its geometric properties, which are determined by the geometry the point forms with its neighbouring points. The result is the identification of homogenous regions in the point cloud, composed of points with similar geometric properties [8]. For the purpose of rock mass characterisation similar geometric properties are equivalent to the membership to the same planar structure or discontinuity. The main advantage of point cloud segmentation is that surface reconstruction is not required and the original point cloud data is used. Consequently, there is no loss in data and less computing power is necessary [4]. For the point cloud segmentation edge-based and bottom up region-based methods are generally used for identifying simple geometric objects like planes. The edge-based method finds edges in the point cloud and classifies points within the developing shapes with the same label. This approach is rather sensitive to noise and uneven point cloud densities, which are common properties of laserscan data from geologic outcrops. The bottom up region-based method starts with a seedpoint, from which a growing process is initiated, until the geometric properties differ. This approach is more robust to noise, however sensitive to the location of the initial seedpoint and tends to inaccuracies near discontinuity boundaries [8] [9]. For rock mass characterisation this method is described by Slob (2007) who uses the bottom up region-based approach to label points belonging to the same planar structure with identical labels. The basic principle is that a random seed point is selected from the point cloud and its k-nearest neighbours are searched. Then a planarity criterion is carried out on this subset of points. The most common algorithm for this planarity criterion is the Principal Component Analysis (PCA), which determines the degree of planarity and the normal vector of the best fit plane. If the planarity criterion is fulfilled the points are labelled with the same integer value and new seedpoints on the edge of the subset are selected. This procedure continues and the plane grows, until the planarity condition fails. Then a new random seedpoint is selected and the label increases with the value of one. Eventually each point of the point cloud is labelled with an integer number describing its membership to a plane and the plane normal vector is obtained giving the plane's orientation [5]. This approach is followed in this thesis for the semi-automatic methodology (section 5.1.2). Other authors such as Jaboyedoff et al. (2007), Gigli & Casagli (2011), Riquelme et al.

(2014), Buyer & Schubert (2016) and Guo et al. (2017) follow a similar approach but resign from the process of growing planes. Instead the normal vector orientation of every point of the point cloud, which fulfils the planarity criterion, is recorded. This method is implemented in various software like DSE (Discontinuity Set Extractor) [10], DiAna [11] and Coltop 3D [9].

There is general agreement among authors on the depiction of the obtained orientation data. The Kernel Density Estimation (KDE) is used to depict the densities of calculated normal vectors, which are displayed in a stereographic projection. KDE is a non-parametric probability density function, which means the distribution shape is only dependent on the data itself. A smoothing parameter distinguishes it from usual histograms [10]. The KDE is suitable for displaying the density for millions of normal vector measurements. From the KDE density peaks can be detected, which serve as starting points for the clustering analysis.

To eventually assign each point to a discontinuity set and calculate discontinuity set parameters like mean orientation and Fisher-k value, clustering algorithms are executed. Various algorithms for instance DBSCAN [10], Fuzzy k-means [7] [5] [6] or Firefly and Fuzzy-c means [4] are implemented for this purpose by different authors.

### 3. Data

#### 3.1. Field of work

The processed laser scans were recorded in the surroundings of the town Kaili, which is the metropolis of the autonomous region Qiandongnan, in the southeast of the Chinese province Guizhou (figure 1). As already multiple rockfalls have occurred in this area, an extensive analysis of the kinematic stability is a matter of particular interest.



figure 1: The geographic location of Kaili, in the southeast of China, is tagged in the image. (bing.com/maps)

The investigated lithology is limestone. Karst phenomena and dissolution processes clearly play a vital role when it comes to failure in this particular area. Dissolution increases the discontinuity size, persistence and connectivity, which leads to a permanent decrease in resisting forces. Often episodically acting factors, like heavy rainfall or earthquakes, finally trigger the rockfall. Water acts as a trigger due to seepage forces acting downward, or buoyancy forces in water-saturated fractures, leading to a decrease of normal stresses and a consequent drop in shear strength. In the lower aerial photography of figure 2 a sinkhole,

which most likely contributed to the failure, by allowing more water to infiltrate the rock mass, is visible. In figure 3 a hole in the upper part of the face is witnessed. It is most likely connected to the sinkhole and was created by continuous dissolution, which weakened the rock mass. This feature may have contributed to a saturation of the failure planes and triggered the rock fall.



figure 2: The two aerial photos show the outcrop Long Chang. The upper photo was taken before, the lower photo after the rock fall event. The sinkhole in the upper middle of the lower photo is clearly visible and indicates high karst activity.



figure 3: The hole in the middle part of the photography, taken at the outcrop Long Chang, was created by karst processes and led to the infiltration of water into the rock mass.

In the photography of figure 4 the persistent, relatively horizontal bedding plane and multiple sub-vertical fractures are clearly visible. The determination of the accurate orientation of the discontinuities is the aim of this thesis. As the high karst erosion rates altered the face and created rounded shapes, the discontinuity set identification could turn out to be more difficult. Due to karst processes, it is likely that random orientations are witnessed, which do not represent a certain fracture set but are created by dissolution.



figure 4: The photography shows the Long Chang outcrop. The reddish area is freshly exposed by the rockfall event. The sub-horizontal bedding and multiple sub-vertical fracture sets are observed.

### 3.2. Data size and resolution

The data incorporates three laserscans of the locations Long Chang, Xiang Qi Jiang Kou and Lao Hu Po coalmine. As parts of the data have very low point densities or include noise, primarily vegetation, it is first manually cropped with the segmentation tool of the software CloudCompare to extract areas of higher and more constant point density. This results in three point clouds, ranging between 1.5 and 4 million points each. The point densities are generally low and fluctuating between 20 and 100 points/m<sup>2</sup>. Both the low point density and the variability in point density in the data, may affect the result and possible biases must be taken into account.

Varying point densities occur due to the position of the scanner regarding the outcrop face, while data acquisition. Normally multiple scanner positions are used. Linearly stacked scanner positions lead to a lower point density on planes approaching subparallel orientation to the scanner's line of sight. This bias is known as the line of sight or occlusion bias [12]. As the scanner is normally placed perpendicular to the outcrop face, planes normal to the face have the lowest densities and might be underrepresented in the point cloud and consequently in the result. This instance is contrary to the Terzaghi bias (orientation bias) in scan line surveys, where discontinuities normal to the scanline orientation, therefore perpendicular to the face, are intersected more often in relation to discontinuities subparallel to the face and are consequently overrepresented [13].

M. Sturzenegger & D. Stead (2008) describe a scale or resolution bias in point cloud data of low point density, which leads to a shift in set orientation or a complete neglecting of sets. Discontinuity sets with a small persistence compared to the point spacing are overlooked [14]. For discontinuities to be detected it is necessary that their size is significantly greater than the point spacing of the point cloud. In this data, for a point density of approximately 75 points per m<sup>2</sup> and the fact that at least 25 points are necessary for the plane algorithm to detect a plane, every object smaller than 0.3 m<sup>2</sup> cannot be detected. This bias is similar to the truncation bias in scanline surveys, where traces below a certain length are neglected [15]. It is only dependent on the data resolution and can be prevented by using a higher point density.

For the data in this thesis both the line of sight and the resolution bias can be relevant. They both rather affect planes perpendicular to the face (figure 5), as these are usually smaller than the planes forming the overall face orientation and have lower point densities. An overrepresentation of the face orientation and a possible neglect of discontinuity sets perpendicular to the face could tamper the results and must therefore be considered.



figure 5: This unprocessed point cloud of the outcrop Long Chang shows the variability in point density, dependent on the surface orientation. Horizontal and vertical traces with low densities, perpendicular to the overall face orientation are witnessed. A combination of line of sight bias and resolution bias could lead to a neglect of these sets.

## 4. Aim of the work

The primary aim of this work is the implementation of various algorithms, using the software MATLAB, which allow a semi-automatic determination of discontinuity set orientations from a raw 3D point cloud. The semi-automatic approach implies as little human assistance as possible, to increase reproducibility and economic efficiency and decrease human bias. A further advantage is the capability of processing big data volume.

As mentioned in section 2.2. this topic has been of interest for research in engineering geology. The direct point cloud segmentation is an effective method which has been implemented by multiple authors [3] [4] [5] [9] [10] [11] due to the relatively simple implementation and the delivery of good results. For these reasons it is also used in this work for the implementation of the semi-automatic methodology.

Most authors [3] [4] [9] [10] [11] compute the normal vector orientation of each point of the point cloud (section 5.1.1.1.) and display their density distribution in a stereographic projection, using the Kernel Density Estimation (section 5.1.2.2.). This way discontinuity sets, which consist of large planes with high point densities, are overrepresented. Discontinuity sets consisting of smaller planes with a lower point density therefore might be missed. Due to the line of sight bias, discussed in section 3.2., discontinuities perpendicular to the face orientation often have lower point densities. Furthermore, the same discontinuities are usually smaller compared to those that form the overall face orientation. This combination can lead to discontinuity sets perpendicular to the face being overlooked, as they are too small compared to the point spacing. This instance is described by the resolution bias in section 3.2.

In this thesis better results are expected when growing planes from the points of the point cloud (section 5.1.2.1.) and using one normal vector measurement for each grown plane. This approach is described by Slob (2007). With this procedure small planes or planes with low point densities affect the results equally as larger planes or planes with higher point densities. This method may decrease the overrepresentation of the face orientation and allow discontinuity sets perpendicular to the face to be detected more reliably. The implementation of the algorithms for the semi-automatic methodology is explained in detail in section 5.1.2.

For testing the algorithms, three point clouds captured in Kaili, China (section 3) are processed with the semi-automatic methodology and a supervised methodology, which is based on the thorough and time intensive assessment of a geologist. The results of the supervised approach serve for comparison to evaluate the accuracy of the semi-automatic methodology. The supervised methodology is expected to deliver robust results, which are however partly subjective due to the editors' influence.

A secondary aim of the thesis is a simple semi-kinematic stability analysis. It is executed with the orientation data obtained by both methodologies. Three failure modes planar sliding, wedge sliding and toppling are investigated only by considering the orientations of the discontinuities relative to the face orientation. This analysis is a rough estimate which does not consider further discontinuity set parameters such as size, persistence, connectivity and roughness.

## 5. Discontinuity set orientations

### 5.1. Methodology

#### 5.1.1. Supervised methodology

This section describes the supervised methodology for the extraction of structural information from point cloud data using the software CloudCompare, Riegel's RiSCAN PRO and Rocscience's Dips 7.0. The work process consists of four steps. First the point normal vectors are computed, using the software CloudCompare. Secondly the point cloud is segmented in sub point clouds, which represent the single discontinuity sets by using CloudCompare's interactive scalar field filter. Then a discontinuity model is established with RiSCAN PRO, by modelling planes through the points of the segmented point clouds. With the Rocscience software Dips the orientations of these planes are depicted, clustered and the eventual set orientations determined.

##### 5.1.1.1. Computation of normal vectors

As unprocessed point cloud data is merely a depiction of points in 3D space, certain calculations are necessary to derive information about the orientation of structures. Various algorithms are used to compute the normal vectors to each point. As the normal vector to a single point is mathematically not reasonable, it is always necessary to include the neighbouring points to compute the orientation. The freeware CloudCompare provides four algorithms to calculate the normal vectors to each point of the dataset. To identify the most accurate method, a point cloud representing three orthogonal planes is modelled and the different algorithms are executed (figure 6). The Hough Transformation proves to be the only method which does not allow errors near corners. All other methods calculate normal vector orientations, which are not represented by any planes, for points close to corners.

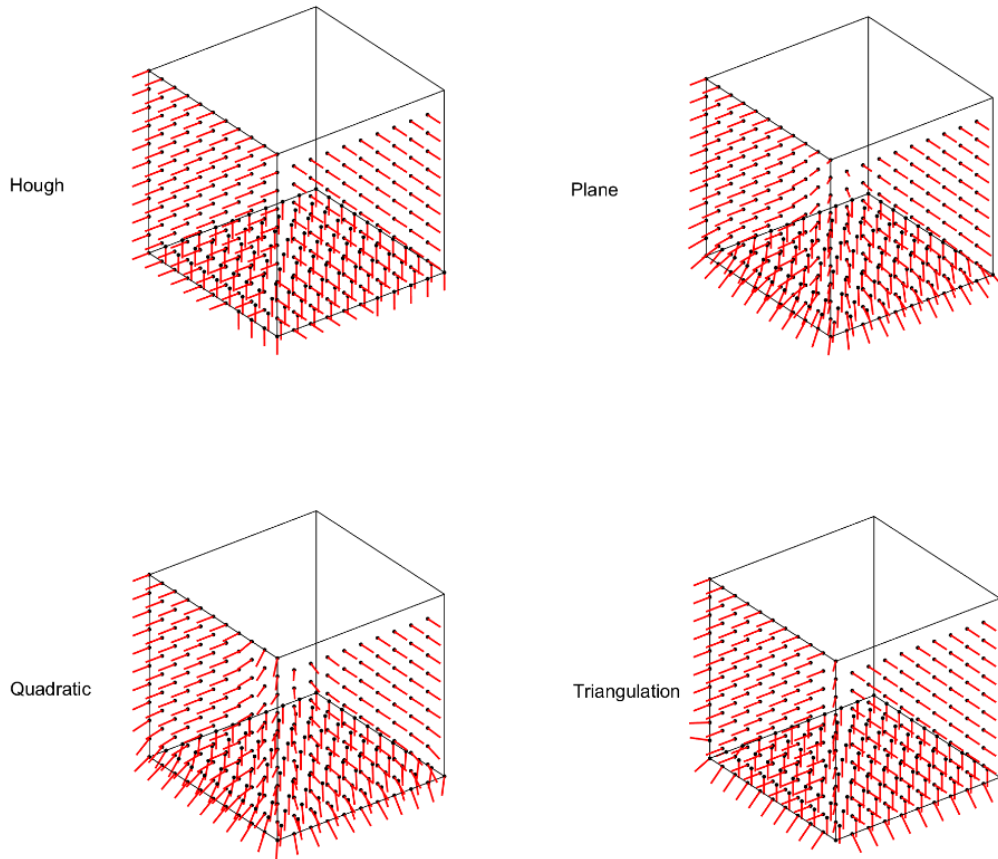


figure 6: The four algorithms of the software CloudCompare, to calculate the normal vector to each point are executed on a model of three perpendicular planes. The red lines represent the orientation of the calculated normal vectors. Only the Hough transformation algorithm (top left) shows correct normal vectors close to edges.

The Hough Transformation is a method which was developed in 1962 to detect lines, circles and other objects in 2D space [16]. The 3D Hough transformation is an enhancement of this method. The principle idea is that an infinite number of possible planes pass through any point. To depict all these potential planes a transformation from 3D cartesian space, described by the parameters  $x$ ,  $y$  and  $z$  to 3D parametric space is performed (figure 7). This space, also called Hough space, is defined by the Euclidean distance from the origin  $\rho$ , the plane normal azimuth  $\theta$  (from  $0^\circ$  to  $360^\circ$ ) and the angle between the plane normal and the horizontal direction  $\phi$  (from  $0^\circ$  to  $90^\circ$ ). The transformation to parameter space follows equation 1 [17].

$$\rho = \sin(\theta) * \cos(\varphi) * x + \cos(\theta) * \cos(\varphi) * y + \sin(\varphi) * z \quad (1)$$

Using the transformation equation, every point of the dataset is described by a sinusoidal curved plane in the parameter space, as shown in the lower images of figure 7. This curve includes all possible planes passing through the point. The intersection of these sinusoidal curved planes in the Hough space indicates a planar structure through these points and displays its plane equation parameters  $\rho$ ,  $\theta$  and  $\phi$ . For indicating discontinuity sets the parameters of the plane normal vector  $\theta$  representing the trend and  $\phi$  representing the plunge, are enough to fully describe the plane orientation. As natural surfaces are not perfectly planar, the parameter space is rasterized in accumulator cells. A threshold value defines a minimum of planes passing through a cell in parameter space to represent a plane [17].

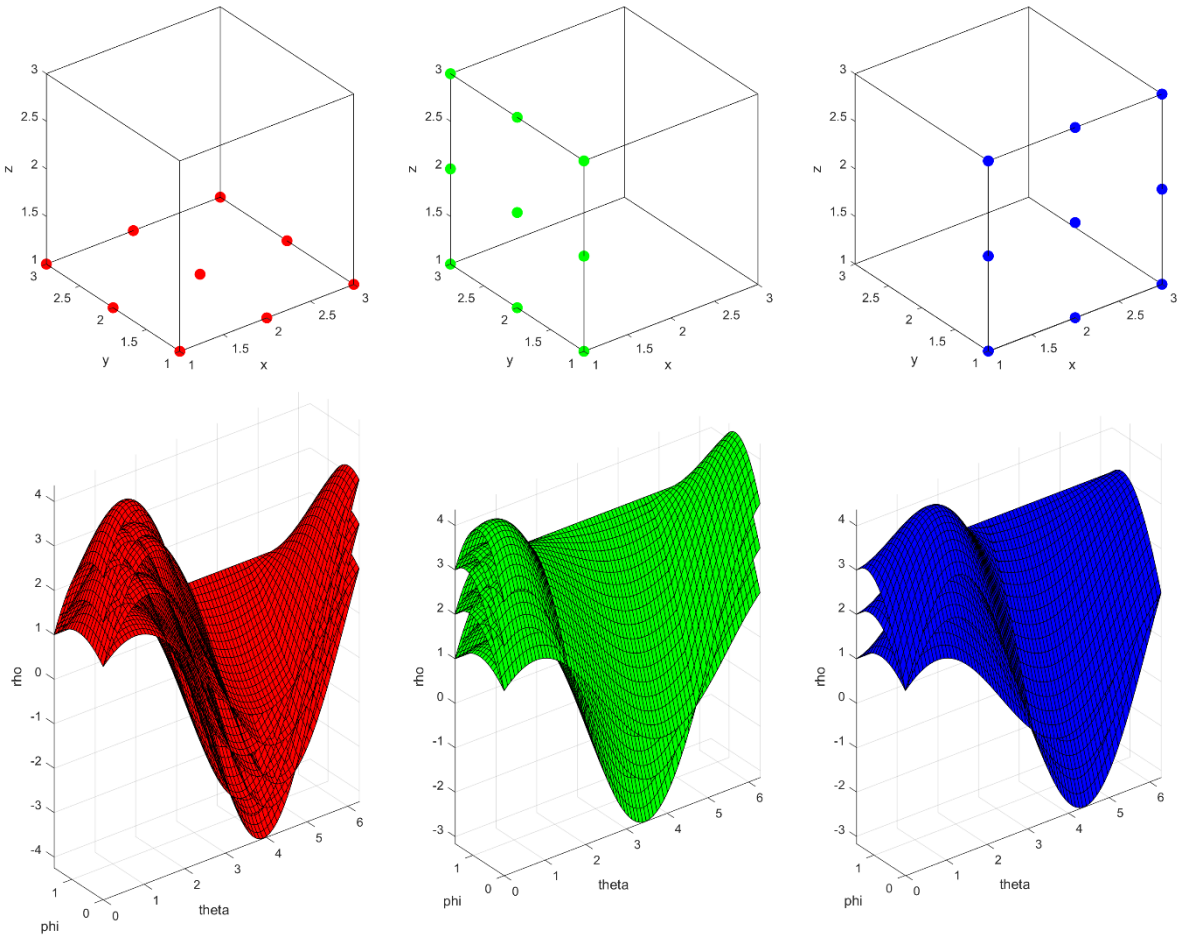


figure 7: The three planes, in the upper images, displayed in cartesian coordinates, are defined by the parameters  $x$ ,  $y$ ,  $z$ . In the lower images the points are transformed into Hough space, defined by the parameters  $\phi$  (angle between plane normal and horizontal direction),  $\theta$  (azimuth of plane normal) and  $\rho$  (distance to the origin). In Hough space all possible planes through a point are displayed by a sinusoidal curved plane. The intersections of planes in Hough space indicate points lying on one plane in the cartesian coordinate system. The  $\phi$  and  $\theta$  axes in the lower image are labelled in radiant.

The example in figure 7 shows three planes consisting of six points each in the upper images. The planes are converted into Hough space in the lower images. The axes are labelled in radiant. The six points of the red plane converted in Hough space are depicted by six sinusoidal curved planes. They intersect at a Euclidean distance  $\rho$  of 1, a plunge  $\phi$  of  $90^\circ$  ( $\pi/2$ ) and in this case the whole range of the trend  $\theta$  from  $0^\circ$  to  $360^\circ$  ( $0$  to  $2\pi$ ). Consequently, the normal vector can be declared  $000/90$ . For the green plane  $\rho$  is 1,  $\phi$  is  $0^\circ$  and  $\theta$  is  $90^\circ$  and  $270^\circ$ . The normal vector is  $090/00$ . For the blue plane  $\rho$  is 1,  $\phi$  is  $0^\circ$  and  $\theta$  is  $0^\circ$  and  $180^\circ$ . The normal vector is  $180/00$ .

### 5.1.1.2. Segmentation of the point cloud

With CloudCompare it is possible to convert the calculated plane normal vectors, which include 3D data of xyz coordinates, to the scalar fields dip direction and dip value. Both scalar fields have one value for each point of the point cloud. The points can be coloured according to the scalar fields to display the orientation of the rock face graphically, as shown in the stereographic projections of figure 8.

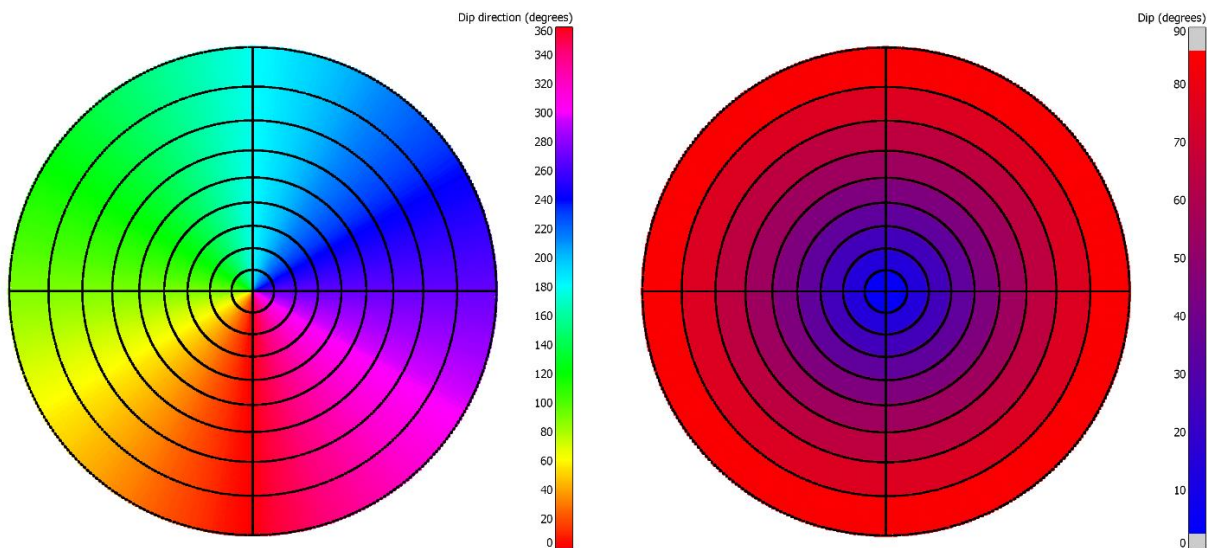


figure 8: In the left stereographic projection, the colour in which the points of the point cloud are depicted when using the dip direction scalar field, dependent on their normal vector trend, is shown. In the right stereographic projection, the colour in which the points are displayed when using the dip value scalar field, dependent on the normal vector plunge, is shown.

The discontinuity set intervals must be defined by a judging geologist, based on the thorough analysis of the point cloud. For the extraction of the individual sets CloudCompare's interactive scalar field filter is a useful tool. It enables the immediate visualisation of the selected boundaries in the point cloud model. The segmented point clouds are the data used for further plane modelling with RiSCAN PRO, as they facilitate the identification and selection of points belonging to one planar feature. Therefore, it is crucial to define reasonable set boundaries for the segmentation as this will influence the result. Each segmented point cloud can be displayed in unique colours in a set model. At this point rough set boundaries are determined but no actual plane measurements have been made.

#### 5.1.1.3. Plane modelling

The segmented point clouds, where each roughly represents a discontinuity set, are imported one at a time into the software RiSCAN PRO. Planes are modelled through the points and the plane orientations are determined. This task can be considered as the equivalent to traditional field measurements of plane orientations. The goal is to obtain reasonable measurements for the further stability analysis. The graphic plane model which is generated with RiSCAN PRO can be compared to the set model, described in the end of section 5.1.1.2., to control the quality of the measured planes.

#### 5.1.1.4. Clustering

For the final determination of the discontinuity set orientations the measurements carried out with RiSCAN PRO are imported into the Rocscience software Dips. It offers the clustering of all measurements, to eventually derive the final set orientations, based on the plane orientation measurements. Further stability analysis is also executed with the software Dips.

### 5.1.2. Semi-automatic methodology

The semi-automatic discontinuity extraction algorithm is fully implemented in MATLAB® (The Mathworks Inc.). A bottom up region based direct point cloud segmentation approach is followed [5] [8] [9]. The procedure consists of three parts. First plane growth starts from a random seedpoint and continues until the planarity criterion is violated. For the planarity criterion the Principal Component Analysis (PCA) is used [18]. Every point is assigned to a discontinuity plane and the plane's normal vector is determined. Secondly, for the identification of the number of discontinuity sets and their rough centres, the Kernel Density Estimation (KDE) displays the density of the plane's normal vectors in a stereographic projection. Eventually a spherical clustering algorithm determines the membership of each point to a certain discontinuity set and identifies the final set centres.

#### 5.1.2.1. Plane growth

The input data is a matrix with  $n$  rows, where  $n$  is the number of points of the point cloud, and three columns of xyz cartesian coordinates to each point ( $[n \times 3]$  matrix). The x coordinate is oriented towards east, the y coordinate towards north and the z coordinate consequently represents the elevation. The first output is a  $[n' \times 7]$  matrix, with  $n' < n$  as some seedpoints fail the planarity condition and are consequently deleted. The seven columns again include the cartesian coordinates xyz of each point in column one to three. Further, a plane index in column four, which assigns each point to a plane, and the three columns five to seven, which contain random integers between 0 and 255 as red, green and blue values (RGB) for each plane index, to enable the depiction of the planes in a plane model, are added. The second output matrix contains one normal vector to each identified plane and the corresponding plane index.

In figure 10 the individual steps of the plane growing algorithm are depicted. The algorithm starts by the selection of a random seedpoint from the input matrix. The next step is the k-nearest neighbours search, which identifies the k points with the smallest Euclidean distance to the seedpoint. In this work the parameter k was set to 25. For the search a k-D tree structure is necessary to provide acceptable computing time. The k-D tree structure divides the space in subspaces along one axis of the coordinate system, to obtain spaces with equal data points. This subdivision is executed multiple times along the three cartesian axis, which

leads to the formation of a tree like structure (figure 9). The searching process then uses this structure and follows the branches to the seedpoint's subspace, instead of executing the search in the hole dataset [6]. Although this method leads to errors on subspace boundaries it is necessary for the computing efficiency. In MATLAB the k-nearest neighbour search, including the establishment of a k-D tree structure is implemented in the function '*knnsearch()*' with the query matrix, the seedpoint and the value for k as input.

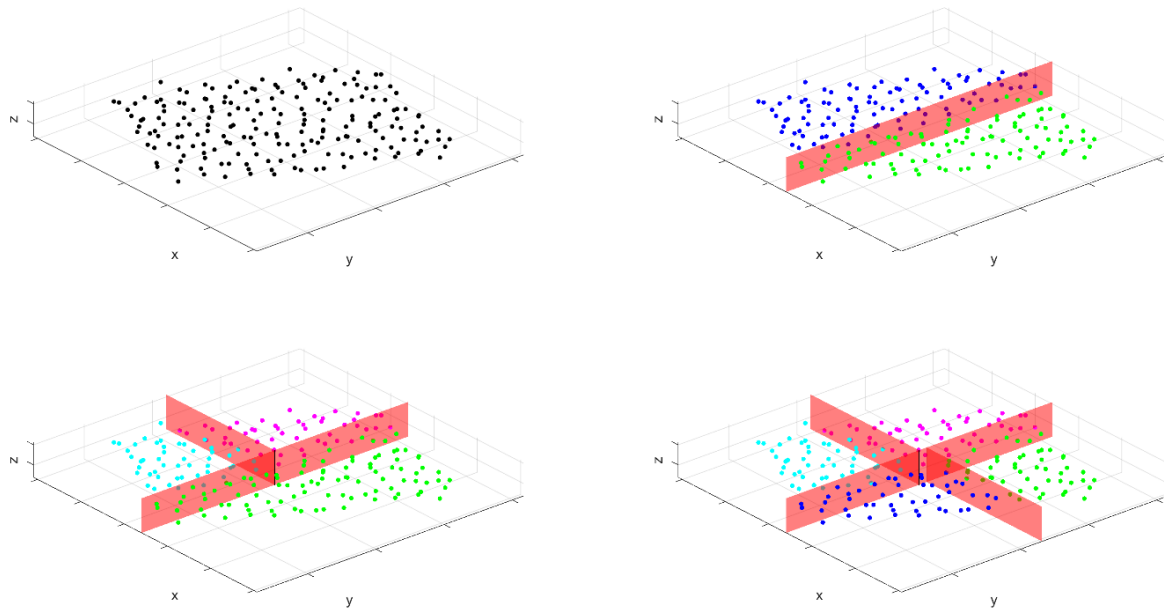


figure 9: The four figures show the process of k-D tree structure development. First the unstructured point cloud (top left) is divided along the x-axis into two subspaces with the same number of points (top right). Then both subspaces are divided along the y-axis again (bottom left and right). In a next step this process would be performed along the z axis.

The result of the nearest neighbour search is a subset of  $k+1$  points, containing the seedpoint and its nearest neighbours. For this subset the planarity analysis is performed. The planarity criterion is based on the Principle Component Analysis (PCA), which is a tool for multivariate data analysis. It geometrically finds the best fit plane to the selected points [18]. This method is equivalent to a least squares solution [9]. It is the most common algorithm for plane detection in geotechnical engineering [4] [5] [9] [10].

First the covariance matrix of the  $k+1$  points of the subset is computed. The covariance matrix is a symmetric matrix (the matrix is equal to the transposed matrix) with the variances as elements of the principal diagonal and covariances as the remaining elements (formula 2). The formulas for the three variances are given in formula 3 to 5. The formulas for the three

covariances are given in formula 6 to 8. In MATLAB the covariance matrix is computed with the function 'cov()' and a [n x 3] matrix (xyz coordinates of the subset's points) as input [19].

$$\begin{bmatrix} var\ x & cov\ xy & cov\ xz \\ cov\ yx & var\ y & cov\ yz \\ cov\ zx & cov\ zy & var\ z \end{bmatrix} \quad (2)$$

$$var\ x = \frac{1}{k+1} \sum_{i=1}^{k+1} [x_i - \bar{x}]^2 \quad (3)$$

$$var\ y = \frac{1}{k+1} \sum_{i=1}^{k+1} [y_i - \bar{y}]^2 \quad (4)$$

$$var\ z = \frac{1}{k+1} \sum_{i=1}^{k+1} [z_i - \bar{z}]^2 \quad (5)$$

$$cov\ xy = cov\ yx = \frac{1}{k+1} \sum_{i=1}^{k+1} [x_i - \bar{x}][y_i - \bar{y}] \quad (6)$$

$$cov\ xz = cov\ zx = \frac{1}{k+1} \sum_{i=1}^{k+1} [x_i - \bar{x}][z_i - \bar{z}] \quad (7)$$

$$cov\ yz = cov\ zy = \frac{1}{k+1} \sum_{i=1}^{k+1} [y_i - \bar{y}][z_i - \bar{z}] \quad (8)$$

From the quadratic [3x3] covariance matrix the Eigenvectors and Eigenvalues are computed. Eigenvectors  $\vec{v}$  are vectors to a quadratic matrix A which are, when multiplied with the matrix, only stretched or compressed but not distorted. The multiplication with this matrix consequently gives the same results as multiplying with a distinct scalar  $\lambda$  (formula 9). This scalar  $\lambda$  is the Eigenvalue and represents the extent of stretching or compressing. When  $\lambda\vec{v}$  is subtracted from this equation it results in a homogeneous linear system of equations. For the subtraction  $\lambda$  is multiplied with the identity matrix I (formula 10).

$$A * \vec{v} = \lambda * \vec{v} \quad (9)$$

$$[A - \lambda * I] * \vec{v} = 0 \quad (10)$$

This system has a non-trivial solution for the Eigenvector only if the matrix  $[A - \lambda I]$  is singular. Consequently, the determinant of this matrix must be zero (formula 11 and 12).

$$\det|A - \lambda * I| = 0 \quad (11)$$

$$\det|A - \lambda * I| = \det \begin{vmatrix} a_{11} - \lambda & a_{12} & a_{13} \\ a_{21} & a_{22} - \lambda & a_{23} \\ a_{31} & a_{32} & a_{33} - \lambda \end{vmatrix} \quad (12)$$

When calculating the determinant of a  $[3 \times 3]$  matrix a polynomial of the third degree, the characteristic polynomial, occurs. By solving the characteristic polynomial, the three Eigenvalues  $\lambda_1, \lambda_2, \lambda_3$  are determined and the Eigenvectors are calculated by solving the homogeneous linear system of equations from formula 10. In MATLAB the Eigenvectors and Eigenvalues are computed with the function `'eig()'` with the covariance matrix as input [6].

Geometrically the Eigenvector with the highest Eigenvalue is the direction of maximum variance, with the Eigenvalue as a magnitude for the variance in this direction. The Eigenvector with the second highest Eigenvalue is perpendicular to the first Eigenvector and is oriented in the direction of the highest variance in this plane. These two vectors span the best fit plane through the data points. The Eigenvector with the smallest Eigenvalue is perpendicular to this plane and describes the planes' normal vector. The planarity condition is derived from the Eigenvalues. A perfect plane would show variances in two directions only, leading to an Eigenvalue of zero for the third Eigenvector. As geologic discontinuities do not form perfect planes the planarity criterion is formulated as a relation between the smallest Eigenvalue and the sum of the three Eigenvalues (formula 13). This relation is denominated as  $\eta$  and must be smaller or equal to a threshold value  $\eta_{max}$  (formula 14) to fulfil the planarity condition [10]. In this implementation  $\eta_{max}$  was set to a value of 0.2 as suggested by Riquelme et al. (2014).  $\eta=0$  means perfect planarity as  $\lambda_3=0$ .  $\eta=0.33$  indicates no planarity as  $\lambda_1=\lambda_2=\lambda_3$ .

$$\eta = \frac{\lambda_3}{\lambda_1 + \lambda_2 + \lambda_3} \quad (13)$$

$$\eta \leq \eta_{max} \quad (14)$$

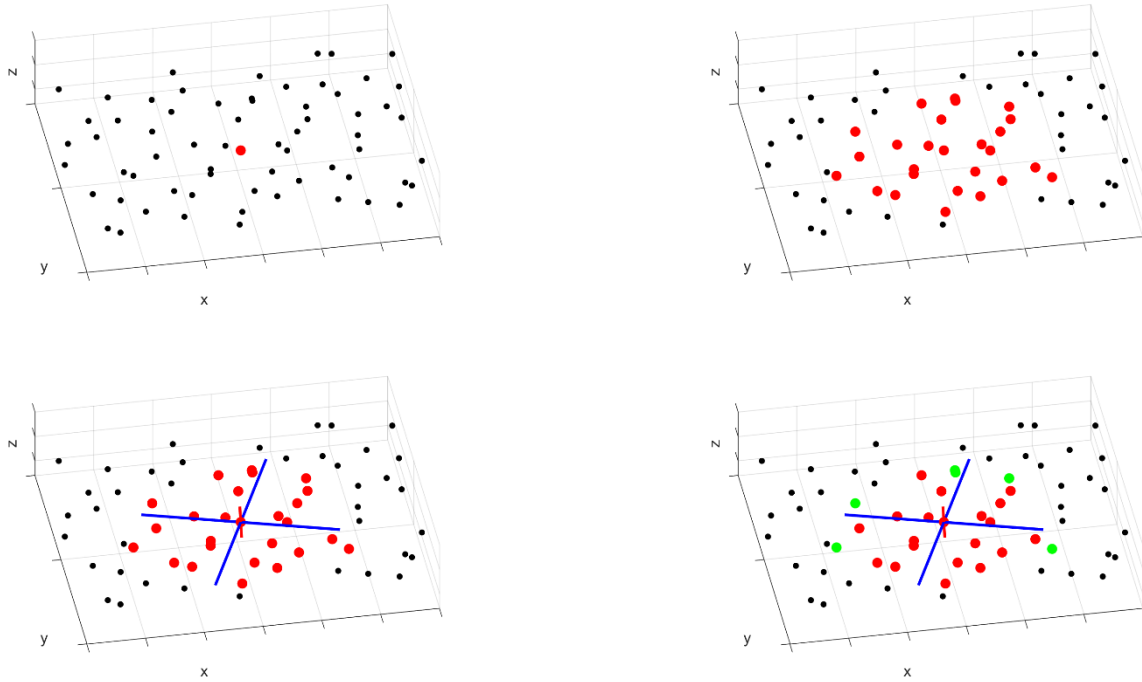


figure 10: The first step in plane growth is the random point selection (red point, top left), followed by the  $k$  nearest neighbour search (red points, top right). Then the Principal Component Analysis (PCA) is executed on the subset of points (bottom left). It determines the first two principal components (blue lines), which span the plane and the third component perpendicular to them (red line), which represents the plane's normal vector. If the planarity criterion is fulfilled, new seedpoints on the edge of the subset are selected (green points, bottom right). This algorithm is repeated, and the plane grows until the planarity criterion is violated.

If the criterion is violated the seedpoint is deleted from the input matrix and a new random seedpoint is selected. If the planarity criterion is valid all points of the subset are stored in the output matrix with a plane index in the fourth column, starting with the integer one, increasing by one for each new plane. Furthermore, the points are deleted from the input matrix. The value of the third Eigenvector, representing the plane's normal vector is stored in a matrix. To enable the growth of the plane new seedpoints on the edge of the subset are selected. In this implementation the five points of the subset with the biggest Euclidean distance to the seedpoint are selected as new seedpoints.

Further, a second criterion is formulated to ensure that the normal vector (third Eigenvector  $\vec{v}_3$ ) of the subset is within a threshold angle  $\varepsilon$  to the average normal vector  $\bar{\vec{v}}_3$ , which is calculated from all normal vectors stored with the same plane index. This criterion is based on the definition of the scalar product of the two unit-vectors  $\vec{v}_3$  and  $\bar{\vec{v}}_3$  (formula 15). In this work  $\varepsilon$  is set at a value of  $20^\circ$ .

$$\arccos\langle \vec{v}_3, \vec{v}_3 \rangle \leq \varepsilon \quad (15)$$

In this manner the plane grows by assigning the same plane index to the points and storing them in the output matrix until one of the two planarity conditions fails. The average normal vector of the plane is calculated from the third Eigenvectors of all subsets and stored in the second output matrix. The plane index rises with the value of one, a new random seedpoint is selected from the input data and the growth of the next plane starts.

This procedure continues until the input matrix is empty, so all points have either been labelled with a plane index or deleted. A third threshold value  $\psi$ , which specifies the limit of points necessary to form a plane, is used in this work. The value is set to 51 points. Points that belong to planes which do not fulfil this criterion are deleted. Eventually each point in the output matrix receives three further columns with equal RGB values for equal plane indices, to depict the planes in unique colours in a plane model.

#### 5.1.2.2. Kernel Density Estimation

The depiction of all plane normal vectors as dots in a stereographic projection leads to an image that is hardly interpretable. For this reason, a density function is established to find the cluster centres. The Kernel Density Estimation is a non-parametric method to estimate a bivariate density function [10]. A non-parametric function shape is not predefined by a parameter but dependent on the data [20]. Contrary to usual histograms the bandwidth (bw.), which is a smoothing parameter, is defined [19]. To compute the KDE the xyz data of the normal vectors must be transformed in xy data of a stereographic projection. The equal angle projection allows the presentation of 3D data in a two-dimensional medium. First the normal vector's xyz data is transformed in its trend  $\alpha$  and plunge  $\beta$ . The geometric relations can be derived from figure 11. For this purpose, first all normal vectors are oriented, pointing in the lower hemisphere of the unit sphere. Therefore, vectors with positive z-values are multiplied with (-1). The trend is calculated with formula 16, the plunge with formula 17.

$$\alpha = \arctan \frac{x}{y} \quad (16)$$

$$\beta = \arcsin|z| \quad (17)$$

When calculating the arc sine of  $z$  its absolute value is used, so positive angles are returned for the plunge. For the calculation of  $\alpha$  a distinction of cases must be made, dependent on the unit circle quadrant, as the arc tangent is used. In the first quadrant formula 16 can be used without modification. In the second quadrant ( $x < 0, y > 0$ )  $2\pi$  is added to the result. In the third ( $x < 0, y < 0$ ) and fourth quadrant ( $x > 0, y < 0$ )  $\pi$  is added.

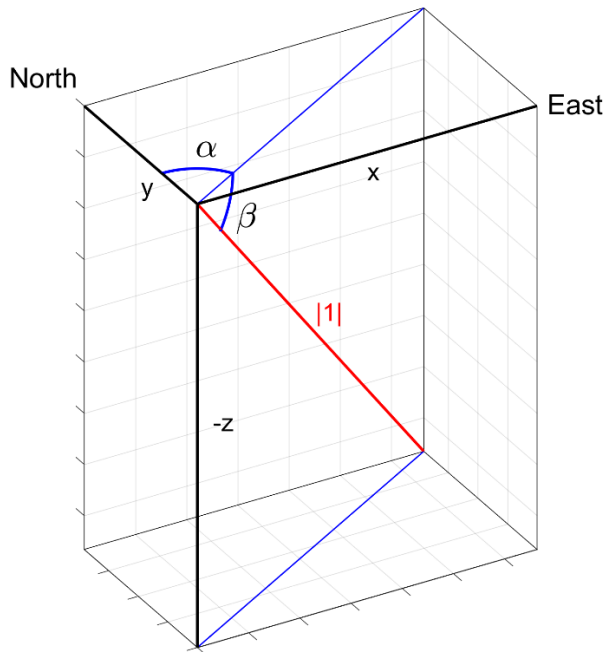


figure 11: This figure exemplifies the correlation between trend  $\alpha$ , plunge  $\beta$  and the 3D coordinates  $xyz$  of the unit vector (red line with the value 1).  $\alpha$  is equal to the arc tangent of  $x$  over  $y$ , while  $\beta$  is only dependent on the  $z$  value and is equal to the arc sine of the absolute value of  $z$ .

The two-dimensional  $xy$  data of the stereographic projection is derived from  $\alpha$  and  $\beta$ . First a transformation of  $\alpha$  and  $\beta$  to the polar coordinates of the stereographic projection  $\theta$ , with values from 0 to  $2\pi$  and the radius  $\rho$ , with values from 0 to 1, is executed. The angle  $\theta$  is equal to the trend  $\alpha$ . In a stereographic projection the projection plane lies on the equator and the projection centre in the zenith. An isosceles triangle forms between the sphere centre, the zenith and the piercing point of the normal vector in the lower hemisphere, as depicted in figure 12. The tangent of the acute angle is equal to the radius  $\rho$  (formula 18).

$$\rho = \tan\left(\frac{\pi}{4} - \frac{\beta}{2}\right) \quad (18)$$

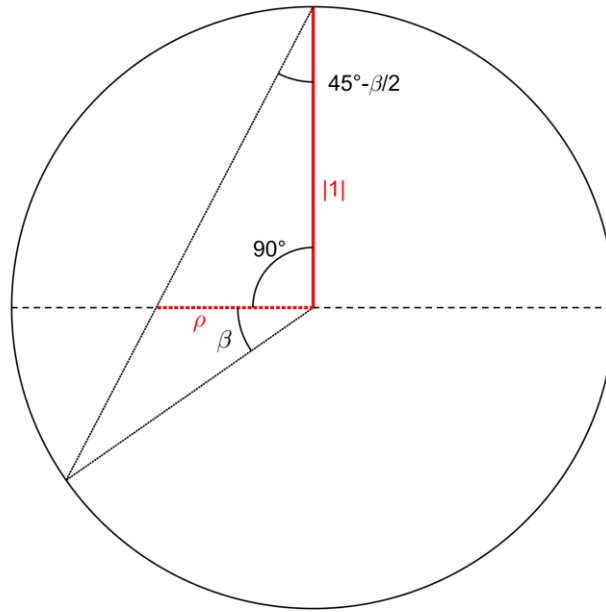


figure 12: This figure illustrates the relation between the plunge  $\beta$  and the radius  $\rho$  in the stereographic projection.

The transformation from polar coordinates to 2D cartesian coordinates follows the simple trigonometric relations from formula 19 and 20.

$$x = \sin(\alpha) \rho \quad (19)$$

$$y = \cos(\alpha) \rho \quad (20)$$

The computed xy coordinates are the input parameters for the Kernel density estimation function. In MATLAB the function '*ksdensity()*' for bivariant data is available and is used for this purpose. The input are the data points' xyz coordinates, a grid of equally spaced points for which the density is calculated and the bandwidth. In this work the bandwidth is set to a value of 0.03. Contour lines with equal probability densities are plotted with the MATLAB function '*contour()*'. The isolines are computed in 1% steps from 1 to 5% and subsequent in 5% steps. The result of the KDE plot is the foundation for the definition of the number of discontinuity sets and allows an estimation of the initial cluster centres for the following clustering analysis.

### 5.1.2.3. Spherical k-means clustering

The k-means clustering algorithm is a relatively fast clustering algorithm but very sensitive to outliers. As the noise has already been eliminated by the planarity criterion the algorithm seems suitable for this task. The standard k-means algorithm consists of two parts. First each data point is assigned to the nearest centroid, using a Euclidean distance criterion. Therefore, not only the number of centroids but also initial centroid positions need to be provided. In the second part the new centroids are calculated from the mean of the assigned data points. This procedure is repeated for a defined number of iterations [21]. The spherical k-means clustering is based on the same principle. Spherical k-means clustering differs in the criterion for the assignment to a cluster. Therefore, a minimum angle between the data vectors  $\vec{n}$  and the centroid  $\vec{c}$  is searched. The aim is to minimize the cosine dissimilarity from formula 21 [21].

$$\sum_{i,j} 1 - \cos(\vec{n}_i, \vec{c}_j) = \sum_{i,j} 1 - \frac{\langle \vec{n}_i, \vec{c}_j \rangle}{|\vec{n}_i| |\vec{c}_j|} \quad (21)$$

When centroids and normal vectors are unit vectors the cosine dissimilarity is simplified to formula 22.

$$\sum_{i,j} 1 - \langle \vec{n}_i, \vec{c}_j \rangle \quad (22)$$

The minimum cosine dissimilarity defines the membership of each normal vector to a centroid. In a second step new cluster centres  $\vec{c}$  are computed, based on the mean of all vectors assigned to this centroid. This vector mean is calculated by dividing the sum of all assigned normal vectors  $\vec{R}$  (formula 24) by the vector's absolute value  $|\vec{R}|$  (formula 23) as in formula 25. By iteration of these two steps the centroids converge to a stable position.

$$|\vec{R}| = \sqrt{\left(\sum n_x\right)^2 + \left(\sum n_y\right)^2 + \left(\sum n_z\right)^2} \quad (23)$$

$$\vec{R} = \sum_i \vec{n}_i \quad (24)$$

$$\vec{c} = \frac{\vec{R}}{|\vec{R}|} \quad (25)$$

A further condition ensures that the newly calculated cluster centres do not deviate more than a defined angle  $\delta$  from the initial cluster centres, to avoid the extensive shift of the estimated set orientations. If the deviation is higher than this angle the shift is reduced to the maximum allowed angle  $\delta$ . The angle  $\delta$  is set to  $5^\circ$  in this thesis.

As input a  $[n \times 3]$  matrix with the computed normal vectors to each plane, the number of iterations of the algorithm, the number of sets  $k$  and a  $[k \times 2]$  matrix with the trend and plunge of the initial centroids, which are estimated from the KDE, are provided. In this work the number of iterations is set to ten. For the clustering the centroid's trend  $\alpha$  and plunge  $\beta$  are transformed in the xyz coordinates of the normal unit-vector in the lower hemisphere, according to the formulas 26, 27 and 28. This transformation is the reversal of the formulas 16 and 17 and the trigonometric correlation can be derived from figure 11.

$$x = \sin(\alpha) * \cos(\beta) \quad (26)$$

$$y = \cos(\alpha) * \cos(\beta) \quad (27)$$

$$z = -\sin(\beta) \quad (28)$$

The output is a  $[n \times 4]$  matrix with the xyz coordinates of the normal vectors and a membership index to a set in the fourth column and a  $[k \times 4]$  matrix with the xyz coordinates of the final centroids and their set indices.

For the correct membership assignment of steep planes and subsequent normal vectors with small plunge, which plot near the edge of the half sphere, the normal vectors are projected in both hemispheres before the cluster analysis. This enables the correct identification of membership for normal vectors that lie on opposing sides of the projection. For the evaluation the cluster centroids of the lower hemisphere are used and those of the upper hemisphere are deleted. All normal vectors are then again oriented in the lower hemisphere, which equals the negative z direction.

The mean set normal vector is already provided by the cluster analysis with the centroid vectors  $\vec{c}$ . Their xyz information is transformed to trend and plunge by formula 16 and 17. The plane dip direction and dip value are calculated from the trend  $\alpha$  and plunge  $\beta$  according to formula 29 and 30.

$$\text{dip direction} = \alpha \pm \pi \quad (29)$$

$$\text{dip value} = \frac{\pi}{2} - \beta \quad (30)$$

The cone of confidence  $\vartheta$  is a value for the reliability of the centre orientation [22]. It can be computed for different confidence levels P and is dependent on the number of normal vectors of the discontinuity set n and their vector sum  $|\vec{R}|$ . In this work confidence levels of 99% (P=0.01) and 95% (P=0.05) are implemented by using formula 31 [22].

$$\vartheta = \arccos \left\{ 1 - \frac{n - |\vec{R}|}{|\vec{R}|} \left[ \left( \frac{1}{P} \right)^{\frac{1}{n-1}} - 1 \right] \right\} \quad (31)$$

A concentration parameter  $k$ , which is a value for preferred orientation, is computed using formula 32. It describes a spherical normal distribution, which is also known as Fisher distribution and therefore is only an approximation for asymmetric distributions [22] [23]. The Fisher- $k$  value is dependent on the number of normal vectors of the set  $n$  and their vector sum  $|\vec{R}|$ . The  $k$  value has big values for high concentrations and small values for low concentrations.

$$k = \frac{n - 1}{n - |\vec{R}|} \quad (32)$$

To depict the  $k$  value graphically the spherical aperture  $\omega$  from formula 33 is calculated.  $\omega$  is a cone's half opening angle and can be depicted as small circle in the stereographic projection [22]. For the assumption of a spherical normal distribution 68% of the discontinuities of a set lie inside the circle. Contrary to the  $k$ -value it has big values for low concentrations and small values for high concentrations.

$$\omega = \arcsin \sqrt{2 \frac{1 - \frac{1}{n}}{k}} \quad (33)$$

## 5.2. Results

### 5.2.1. Supervised methodology

#### 5.2.1.1. Long Chang

Using CloudCompare's graphic depiction of the scalar fields dip direction and dip value and the interactive scalar field filter, six sets are segmented (section 5.1.1.2.). Each set is displayed in unique colours in figure 13 and the sets are merged in figure 14. The used segmentation intervals are listed in table 1.

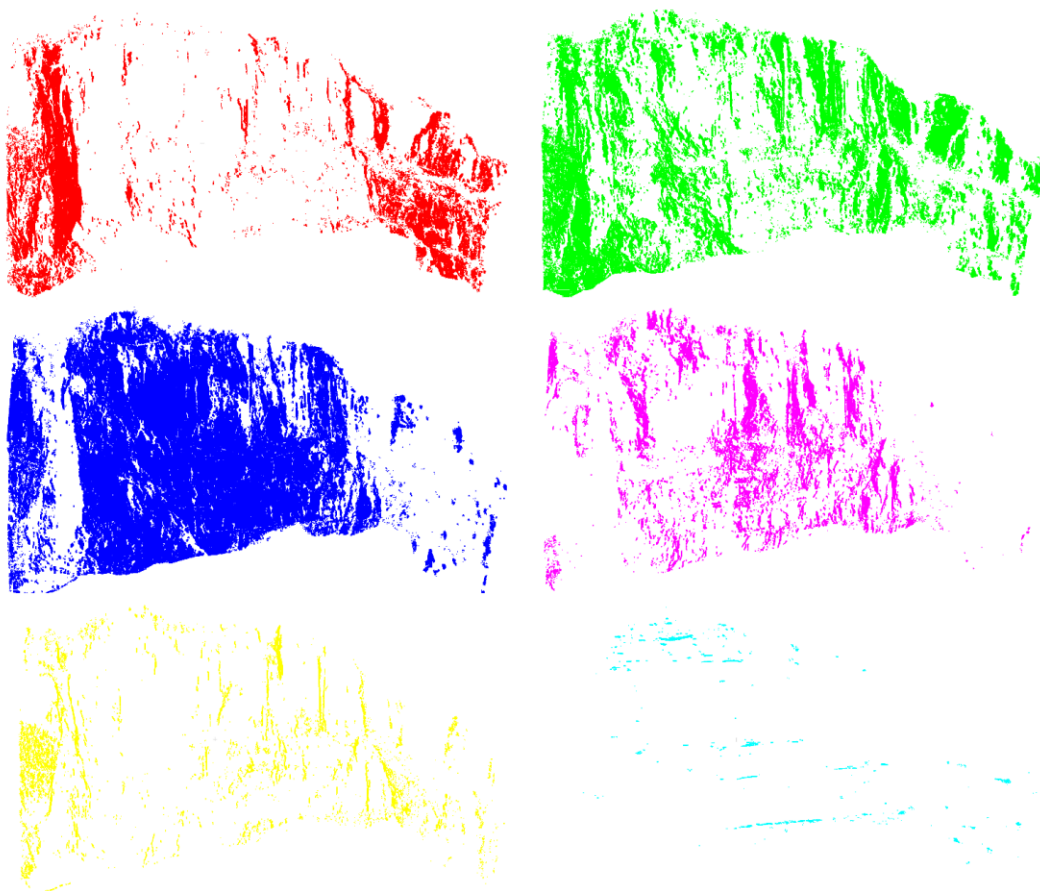


figure 13: The six discontinuity sets of Long Chang, segmented from the original point cloud during the supervised methodology, are displayed in unique colours. The segmentation intervals are determined using CloudCompare's scalar fields dip direction and dip value.

Each segmented discontinuity set is imported in the software RiSCAN PRO, where planes are modelled through the points, and a measurement of each plane is made (figure 15) (section 5.1.1.3). These measurements are imported in the software Dips and a clustering algorithm calculates the average set orientation (figure 16) (section 5.1.1.4.).

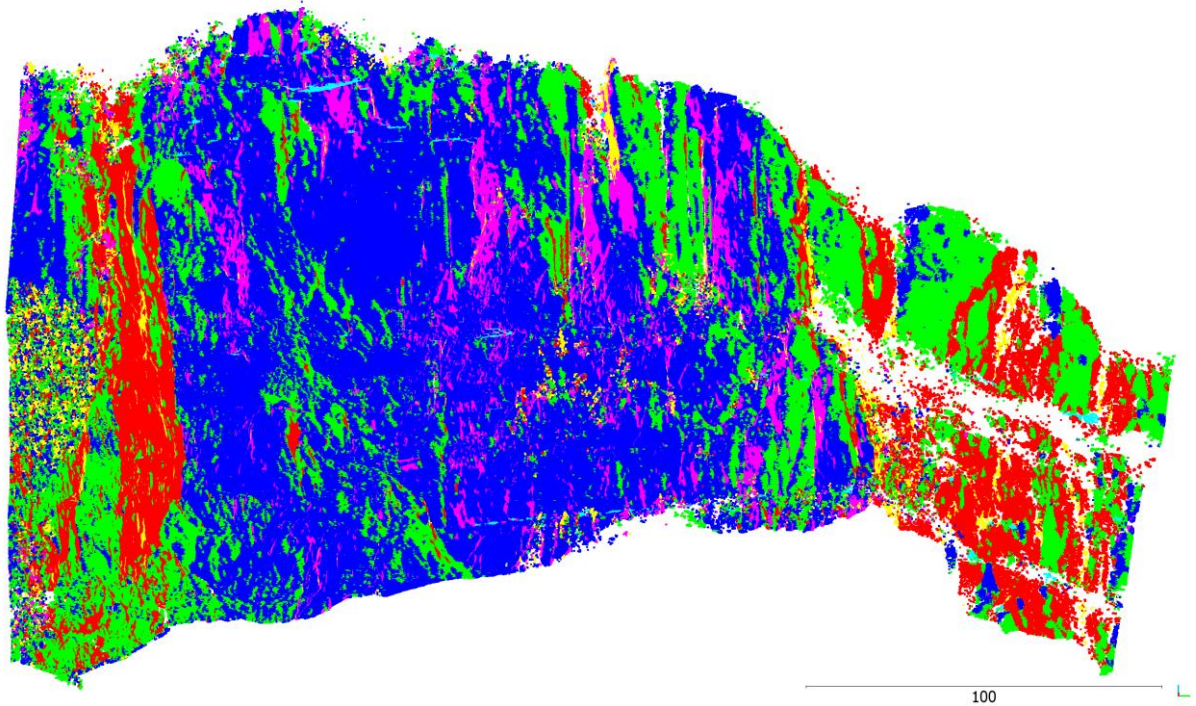


figure 14: The six segmented and uniquely coloured discontinuity sets of the east facing Long Chang outcrop are displayed in the set model obtained from the supervised methodology. It is the merge of the six sets from figure 13.

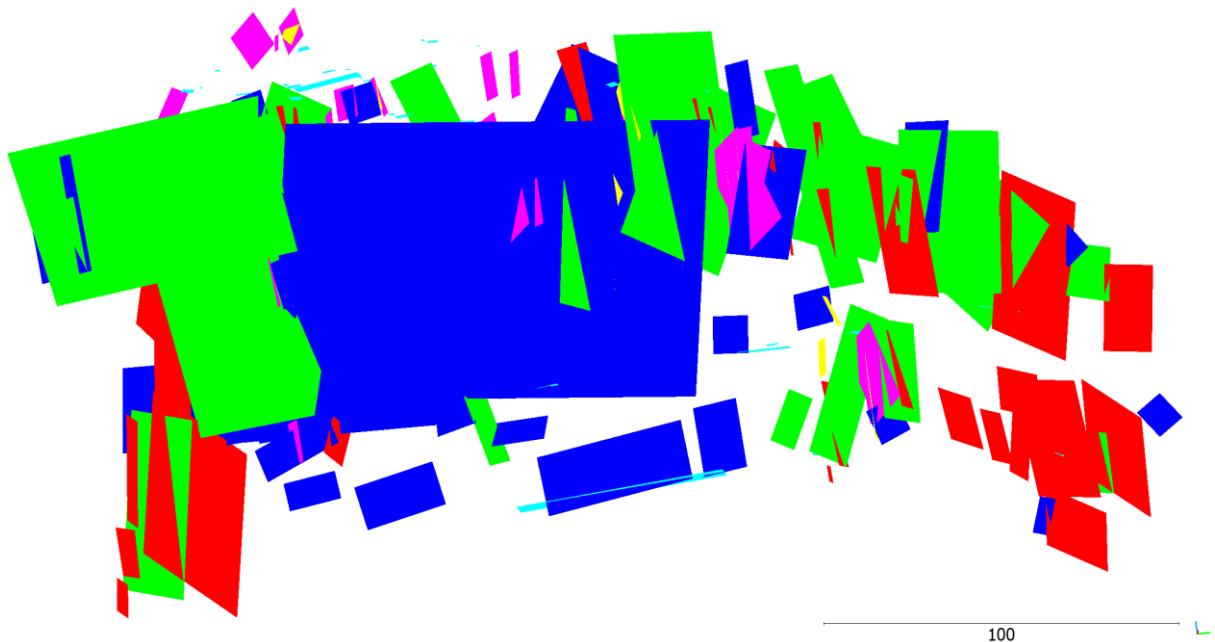


figure 15: The plane model is created with the software RiSCAN PRO. The colours correspond to the colours of the set model in figure 14, the segmented sets in figure 13 and the colours in the stereographic projection of figure 16. One measurement for each plane is made and imported in the software Dips to compute the stereographic projection of figure 16.

table 1: The segmentation intervals of dip direction and dip value, derived during the supervised methodology for the Long Chang data, are listed for each set. The colours correspond to the colours in the set model (figure 14), plane model (figure 15) and stereographic projection (figure 16).

set colour	dip direction	dip value
red	30 – 60 and 210 - 240	40 - 90
green	60 – 93 and 240 - 269	40 - 90
blue	93 – 129 and 269 - 301	40 - 90
magenta	129 – 160 and 301 - 335	40 - 90
yellow	160 – 210 and 340 - 30	40 - 90
cyan	200 - 360	0 - 40

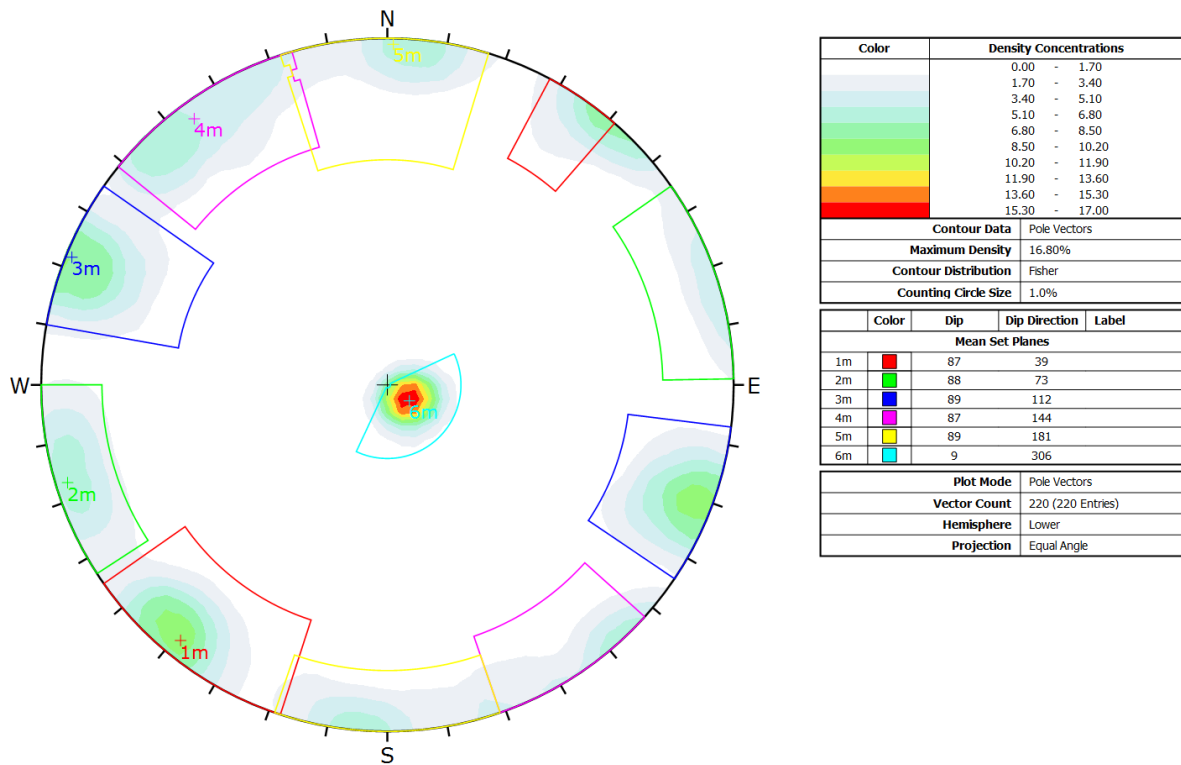


figure 16: The measurements of the planes computed with the software RiSCAN (figure 15) are clustered using the software Dips and ascribed to a discontinuity set. In the right box the mean discontinuity set orientations are listed. The colours of the sets in the projection correspond to the colours of the models in the figures 13 to 15.

### 5.2.1.2. Xiang Qi Jiang Kou

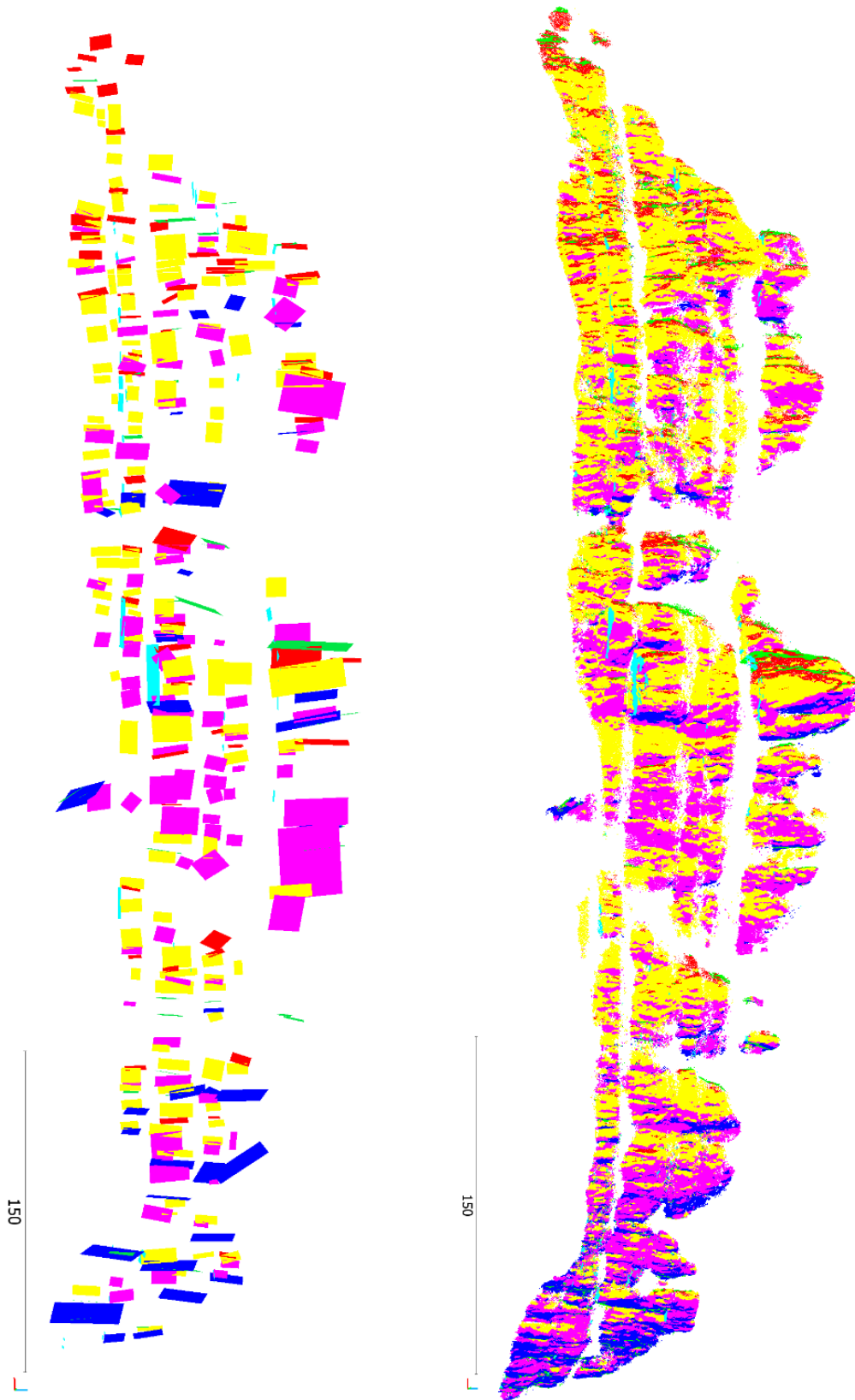


figure 17: The upper figure shows the set model of the north facing Xiang Qi Jiang Kou outcrop received from the supervised methodology. The lower figure depicts the plane model created with RiSCAN PRO. For each plane of the plane model one measurement is made and plotted in the stereographic projection of figure 18. Each discontinuity set is represented by one colour, which coincides with the set colours of table 2 and the stereographic projection in figure 18.

table 2: The segmentation intervals of dip direction and dip value for each set, determined during the supervised methodology for the Xiang Qi Jiang Kou data, are listed in the table.

set colour	dip direction	dip value
red	30 – 60 and 210 - 240	40 - 90
green	60 – 100 and 240 - 280	40 - 90
blue	100 – 130 and 280 - 310	40 - 90
magenta	130 – 165 and 310 - 345	40 - 90
yellow	165 – 210 and 345 - 30	40 - 90
cyan	200 - 360	0 – 40

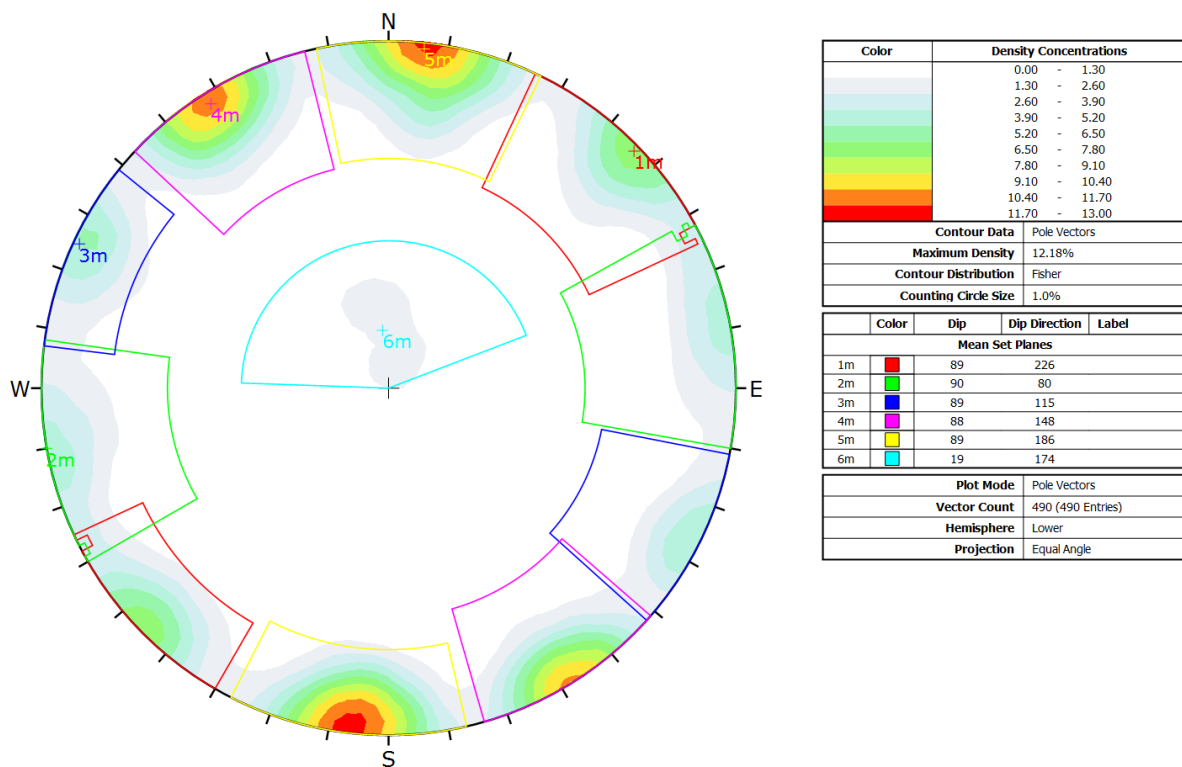


figure 18: The stereographic projection is computed with the software Dips. The orientation data is obtained by measurements of the planes from the plane model in figure 17.

### 5.2.1.3. Lao Hu Po coalmine

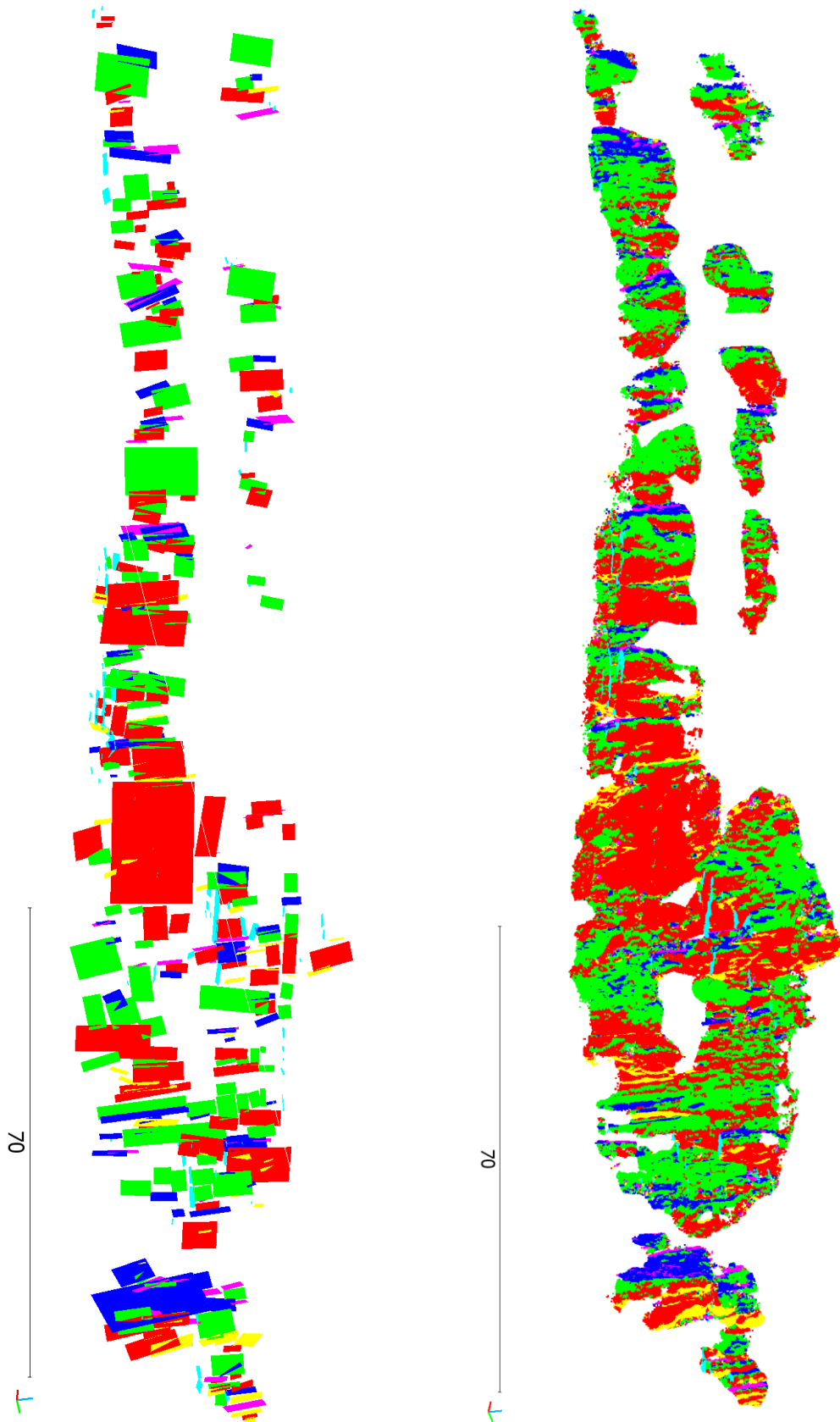


figure 19: The upper figure displays the set model of the northeast facing Lao Hu Po coalmine, computed during the supervised methodology. The lower figure displays the plane model created with the software RiSCAN PRO.

table 3: The segmentation intervals of dip direction and dip value for each set, used for the supervised methodology for the Lao hu Po coalmine data, are listed in the table.

set colour	dip direction	dip value
red	5 – 45 and 185 - 225	40 - 90
green	45 – 75 and 225 - 255	40 - 90
blue	75 – 105 and 255 - 285	40 - 90
magenta	105 – 145 and 285 - 325	40 - 90
yellow	145 – 185 and 325 - 5	40 - 90
cyan	200 - 360	0 - 40

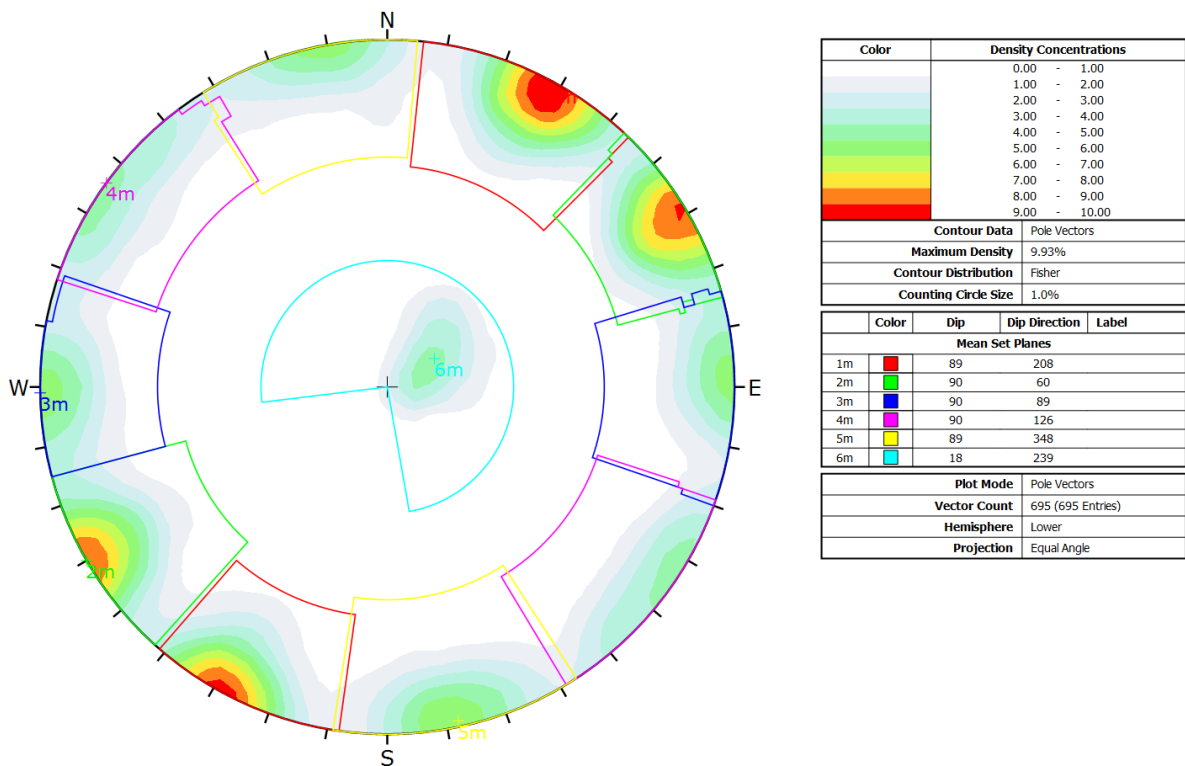


figure 20: The stereographic projection of Lao Hu Po coalmine is computed with the software Dips. The orientation data is obtained by measurements of planes from the plane model, computed with the software RiSCAN PRO (figure 19).

## 5.2.2. Semi-automatic methodology

### 5.2.2.1. Long Chang

For the nearest neighbour search  $k$  is set to 25. For the planarity criterion  $\eta$  is set to 0.2,  $\epsilon$  is set to  $20^\circ$  and  $\psi$  is set to 51 points. The first output of the semi-automatic methodology is a matrix with assigned plane indices to each point of the point cloud. For the depiction of each individual plane in a plane model, random values of red, green and blue between 0 and 255 are computed for every plane index. All computed planes for Long Chang are displayed in figure 21. Further the normal vector of each plane is calculated, as the vector mean of the normal vectors of all points with the same plane index (section 5.1.2.1).



figure 21: In the plane model of the semi-automatic methodology for Long Chang each plane, which fulfils the planarity conditions, is displayed in one colour.

The computed 3D normal vectors are transformed in 2D coordinates of the stereographic projection and the Kernel Density Estimation (section 5.1.2.2) is computed (figure 22) to define the number of sets and the starting centroids for the following clustering analysis. A bandwidth of 0.03 is used and isolines are drawn in 1% steps from 1 to 5% and in 5% steps from 5 to 95%. The highest densities in figure 22, coloured in red, represent the discontinuity set parallel to the face, which is oriented east southeast. Sets perpendicular are strongly underrepresented. From the KDE six sets are determined. Their normal vectors are listed in table 4.

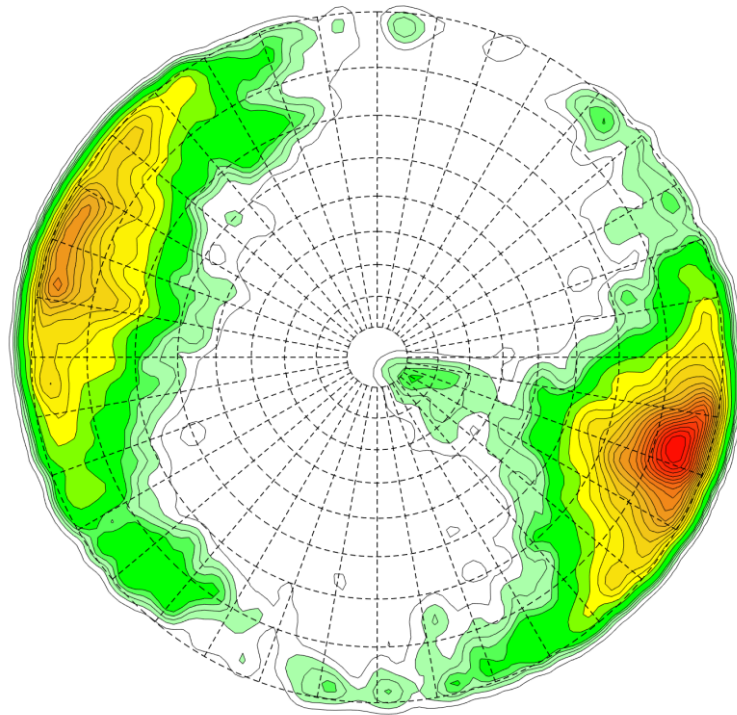
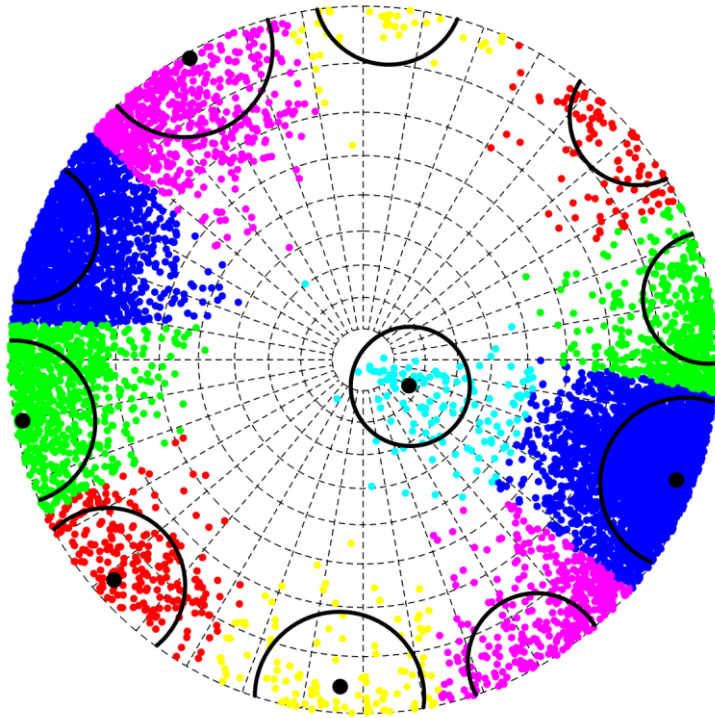


figure 22: The Kernel density estimation displays a probability density function of the computed normal vectors of each plane. Isolines of 1% steps from 1 to 5% and subsequent 5% steps are drawn to optimally visualise density peaks. Additionally, higher densities are coloured in red, whereas lower densities are coloured green.

table 4: The table lists the six initial centroids for the cluster analysis, determined based on the Kernel Density Estimation.

set	trend	plunge
1	005	00
2	045	00
3	075	00
4	108	00
5	155	00
6	120	78

For the clustering analysis (section 5.1.2.3) the initial centroids from table 4 are used and the number of runs is set to 10. The results are plotted in the stereographic projection of figure 23. The Fisher k-value and the spherical aperture are computed. To each point of the point cloud the same set colour which is used in the stereographic projection is assigned, to create the set model depict in figure 24.



set	colour	dipdirection	dipvalue	k-value
1	red	49	87	39
2	green	80	89	38
3	blue	291	87	33
4	magenta	150	89	33
5	yellow	4	86	32
6	cyan	299	17	19

figure 23: In the stereographic projection every plane normal vector is plotted as a coloured dot, dependent on its ascription to a set by the clustering algorithm. The set centres are depicted as black dots and the spherical aperture (formula 33) is drawn as a black circle. The colours correspond to those of the set model in figure 24.

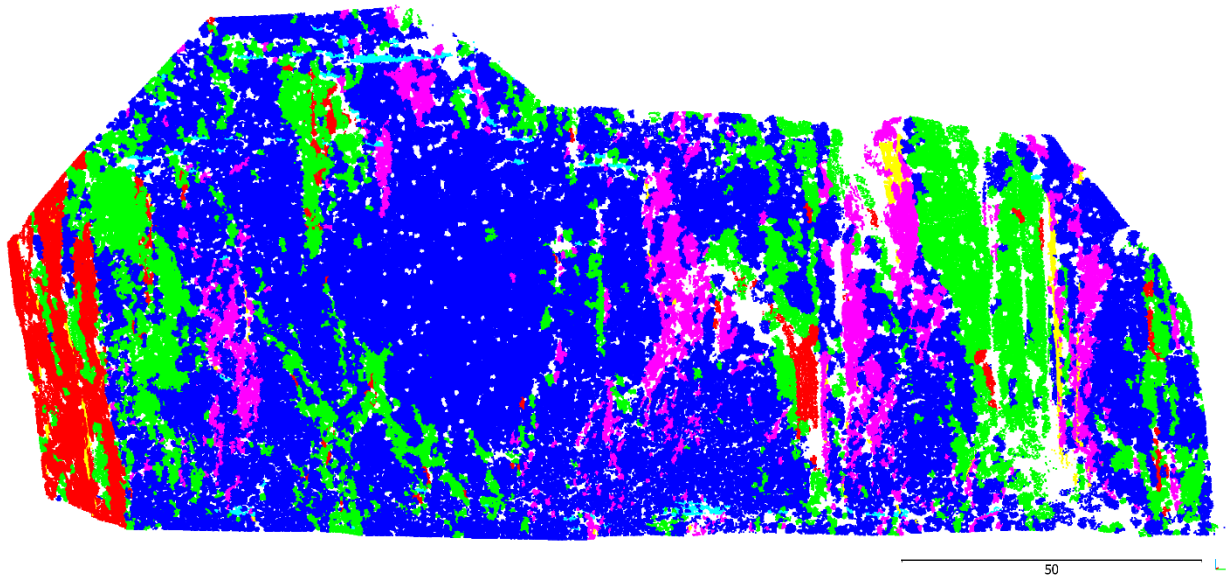


figure 24: The set model of the semi-automatic methodology for Long Chang consists of five-sub vertical sets and a nearly horizontal bedding.

### 5.2.2.2. Xiang Qi Jiang Kou

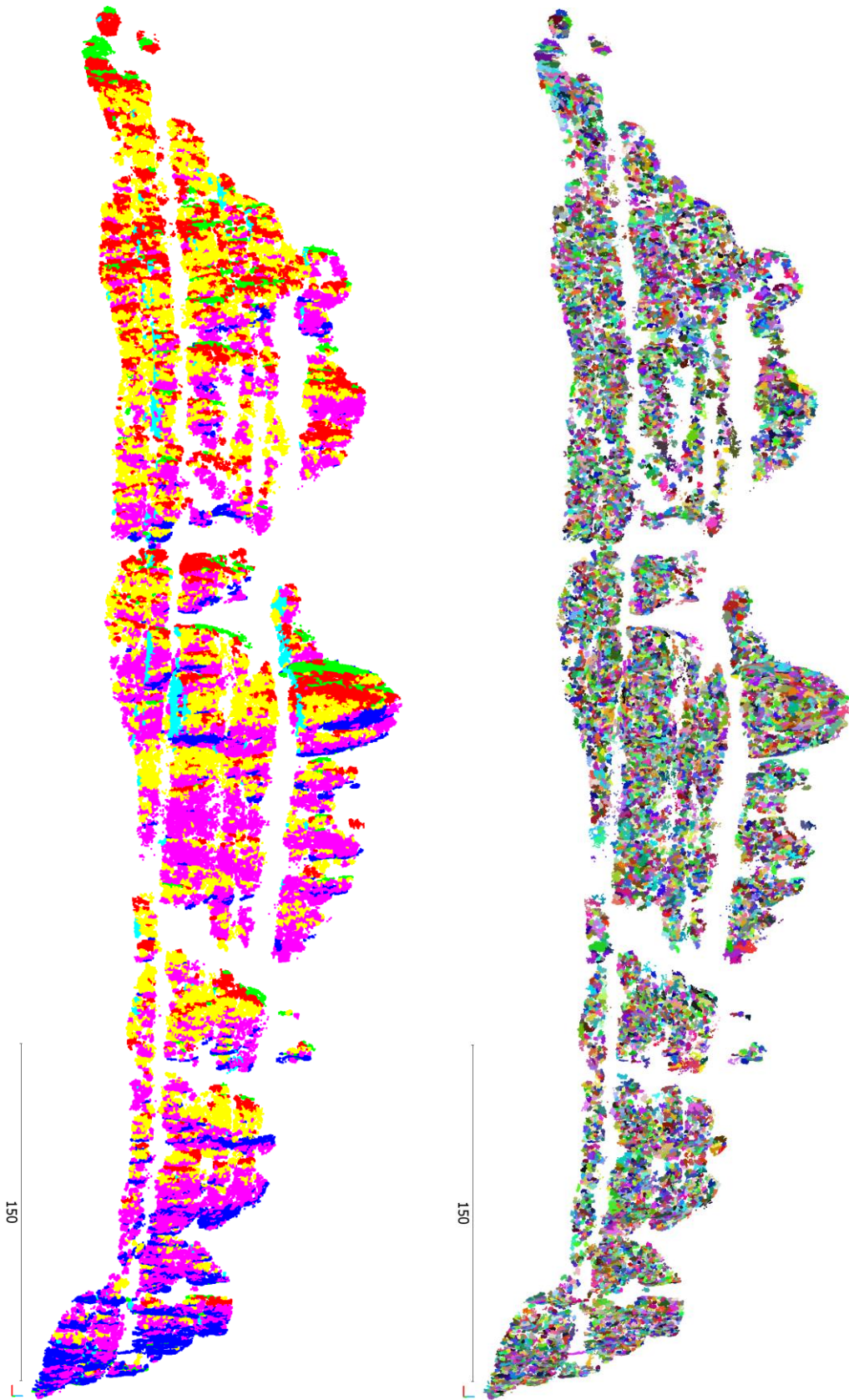


figure 25: The upper figure shows the plane model of Xiang Qi Jiang Kou, computed by the plane growing algorithm during the semi-automatic methodology. The lower set model is created by plotting each point in the colour of the set, the clustering algorithm assigned it to.

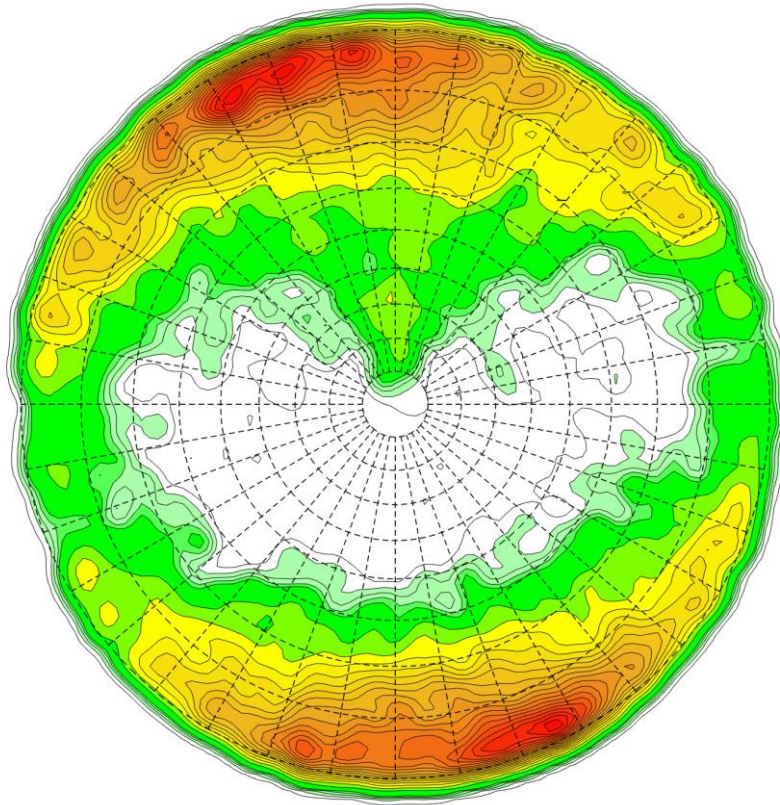
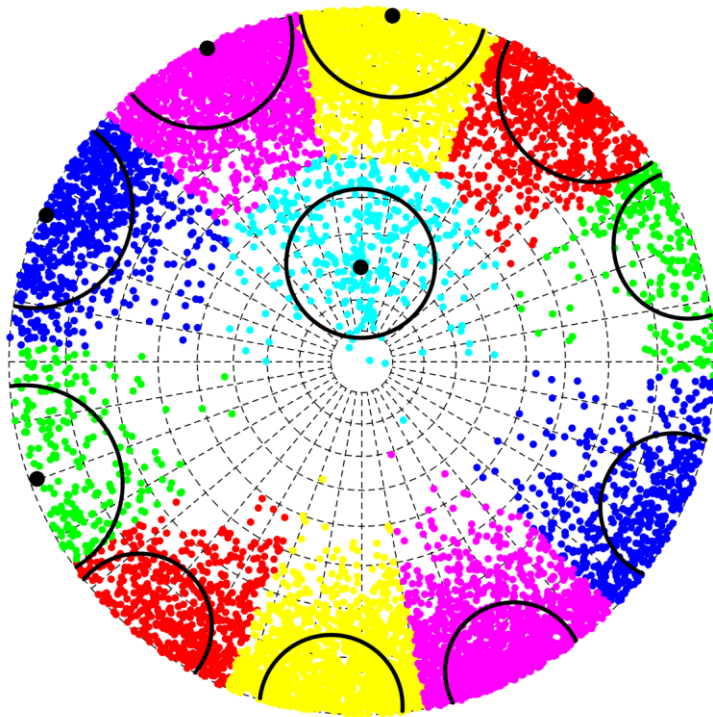


figure 26: The KDE of the normal vectors of each plane, computed during the semi-automatic methodology, for Xiang Qi Jiang Kou, is the foundation for the estimation of cluster centres (table 5) for the clustering analysis. High densities are coloured red, low densities are coloured green.

table 5: In this table the initial set normal vector centres for the cluster analysis are listed. They are estimated based on the KDE in figure 26.

set	trend	plunge
1	010	00
2	045	00
3	075	00
4	110	00
5	155	00
6	000	65



set	colour	dipdirection	dipvalue	k-value
1	red	220	89	28
2	green	70	89	27
3	blue	115	89	27
4	magenta	154	89	32
5	yellow	185	89	29
6	cyan	179	30	14

figure 27: The result of the cluster analysis is the assignment of each point to one discontinuity set. Each set is given a colour for depiction, which corresponds to the colour of the set model in figure 25. Set centres are represented by black dots. The black circles display the spherical aperture (formula 33).

### 5.2.2.3. Lao Hu Po coalmine

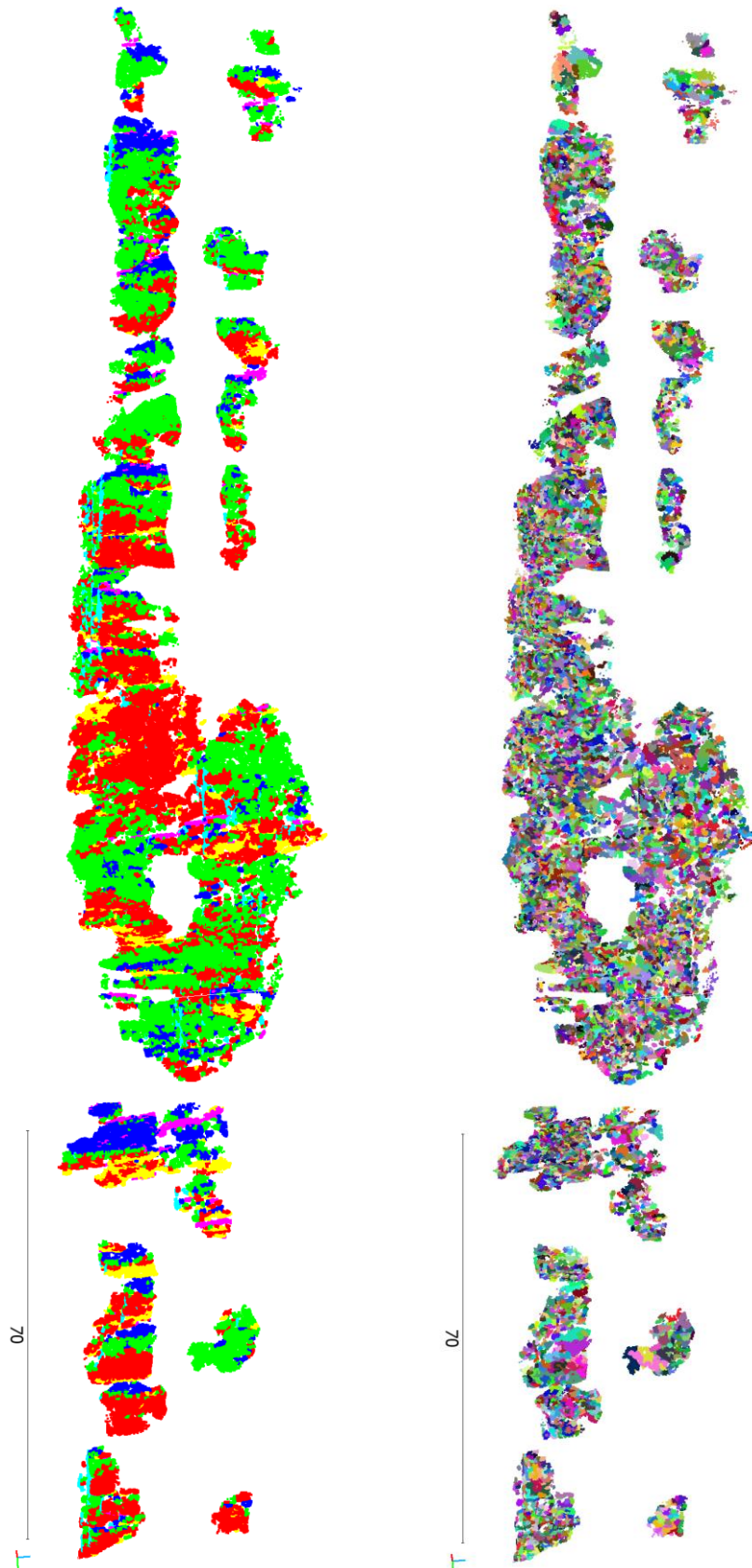


figure 28: The upper figure shows the plane model computed during the semi-automatic methodology for the Lao Hu Po coalmine data. It is created by the plane growing algorithm. The lower figure shows the set model which is obtained from the clustering of the planes and assigning them to distinct sets.

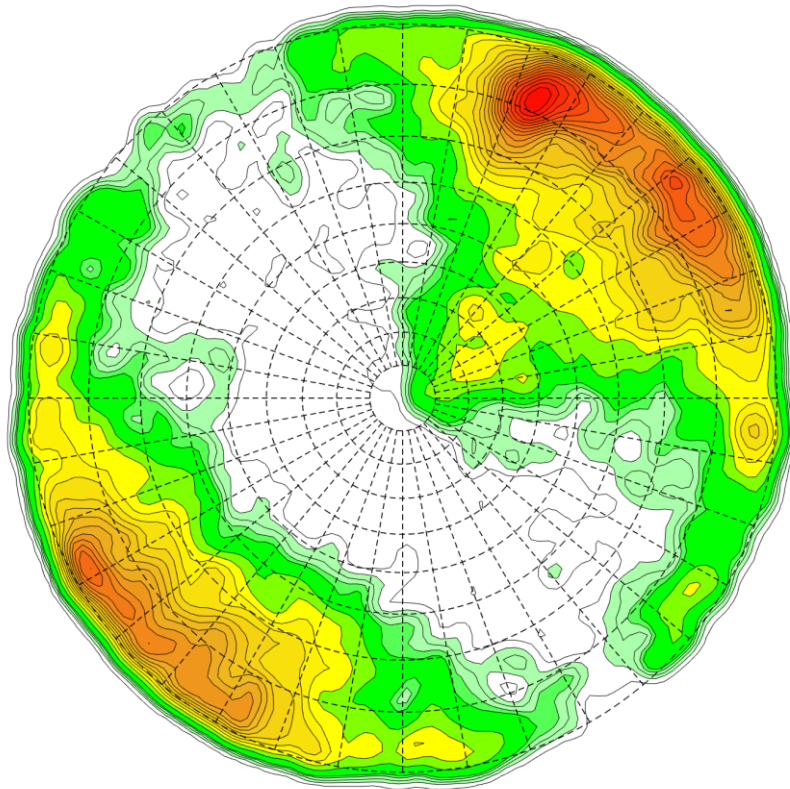
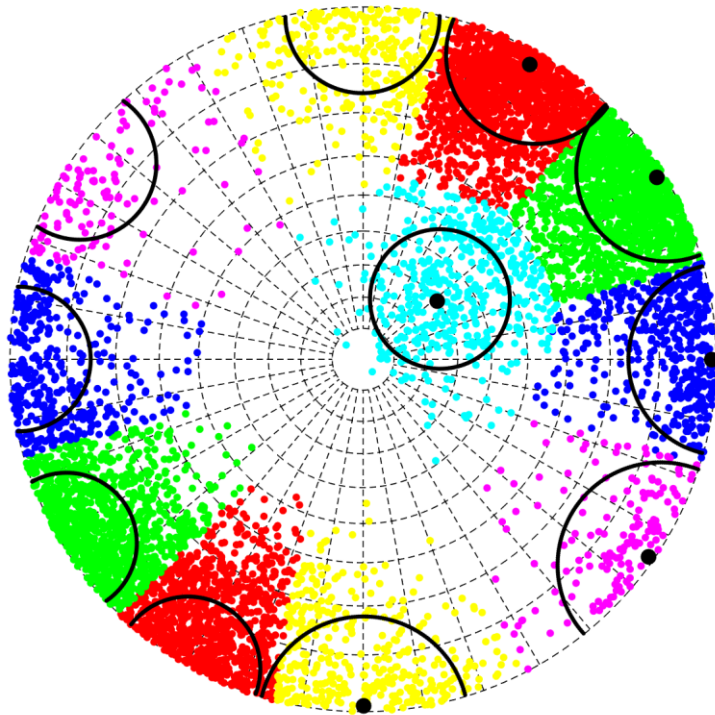


figure 29: The KDE for Lao Hu Po coalmine displays the density distribution of the normal vectors of each plane, computed by the plane growing algorithm, in a stereographic projection. High densities are coloured red, low densities are coloured green.

table 6: In this table the initial set normal vector centres for the cluster analysis are listed. They are estimated based on the KDE in figure 29.

set	trend	plunge
1	025	00
2	055	00
3	095	00
4	125	00
5	175	00
6	050	65



set	colour	dipdirection	dipvalue	k-value
1	red	209	88	31
2	green	238	89	25
3	blue	270	89	24
4	magenta	305	89	16
5	yellow	0	89	31
6	cyan	232	30	28

figure 30: The spherical clustering algorithm assigns each normal vector in the stereographic projection to one set. The average orientation of the set is calculated and depict as black dot. The spherical aperture (formula 33) is derived from the k-value (formula 32) and drawn as black circle.

### 5.3. Comparison of the methodologies

The supervised methodology is a robust methodology, which however requires the working time of a skilled geologist. The modelling of planes with the software RiSCAN PRO is time consuming but necessary to receive plane orientation measurements for the clustering with the software Dips and to eventually derive numerical values for the orientations. The precision and reproducibility of the results is dependent on the person in charge. Especially the task of defining set boundaries, based on the dip value and dip direction scalar fields and the interactive scalar field filter, using CloudCompare, is influenced by the editor, therefore subjective and possibly affected by human bias.

The semi-automatic methodology starts with the plane growing algorithm. This task is time and computing power consuming, however the same applies to the normal vector computation of the supervised methodology. The semi-automatic methodology is favoured from an economical point of view because, apart from the selection of initial cluster centres for the clustering analysis, based on the Kernel Density Estimation, the methodology is fully automatic. Consequently, it only requires computing power instead of a geologist's working time. Further the automatization has the advantage of high reproducibility and is not influenced by human bias. The already mentioned selection of initial cluster centres, which still requires a geologist's judgement, and the random selection of seedpoints during the plane growth, are the only points in time in the work process, at which the reproducibility could be disturbed. In this thesis the random selection of seedpoints did not have a significant impact, as multiple computation of the plane growing algorithm returned similar results. The planarity criterion and the criterion for minimum points of the semi-automatic methodology also remove remaining noise and non-planar structures of the rock mass, which would tamper the results. This becomes obvious by comparing the number of points of the input matrix to the number of points of the output matrix. About 20% of the data points are deleted as they do not fulfil the planarity criteria. When comparing the models in figures 33 to 39, holes of deleted points in the semi-automatic model are witnessed. This ejection leads to a loss of data on the one hand but to an increase of the remaining data quality on the other hand. With the semi-automatic methodology, a multiple of the plane measurements, compared to the supervised methodology, are made.

A further aim of the plane growing algorithm is to achieve a result less biased by the face orientation. As the line of sight bias and the resolution bias (section 3.2) both rather advantage planes parallel to the face, because they are usually bigger and have higher point densities, sets normal to the face could be overlooked. It is assumed that these biases are increased when measurements of the normal vectors of all points of the point cloud are depicted in a stereographic projection, by using a Kernel Density Estimation, like Riquelme et al. (2014) suggests. In this thesis the plane growing algorithm according to Slob (2007) is implemented, where every plane which is grown results in only one measurement. With this methodology planes consisting of few points are weight the same as planes consisting of many. This should lead to an improved detection of small planes of low point densities. In figure 31 two stereographic projections show Kernel Density Estimations of normal vectors for the location Long Chang. The left image shows the KDE computed with the normal vectors of all points of the point cloud, which are calculated during the supervised methodology, using the software CloudCompare (section 5.1.1.1.). The right image shows the KDE computed with the normal vectors of the planes, grown during the semi-automatic methodology (section 5.1.2.1.). The comparison shows slightly better results for the KDE computed with normal vectors obtained by the plane growing. The vertical discontinuity set with dip direction north becomes more distinct in the right image. This confirms the assumption that the plane growing algorithm improves the detection of discontinuity sets perpendicular to the face. The density peak in the left image, with the trend 310 and plunge 65, does not represent a discontinuity set but originates from noise or curved, weathered structures and does not appear in the right image. This attests that noise and non-planar structures are removed efficiently by the planarity criteria of the plane growing algorithm. Furthermore, the clustering algorithm is a lot faster when only one measurement per plane is considered instead of one measurement for each point. From a traditional point of view using measurements of computed planes is the logic approach compared to the use of measurements of each point. It resembles methodologies like scanline surveys where every discontinuity plane is recorded and weight the same independent from its size.

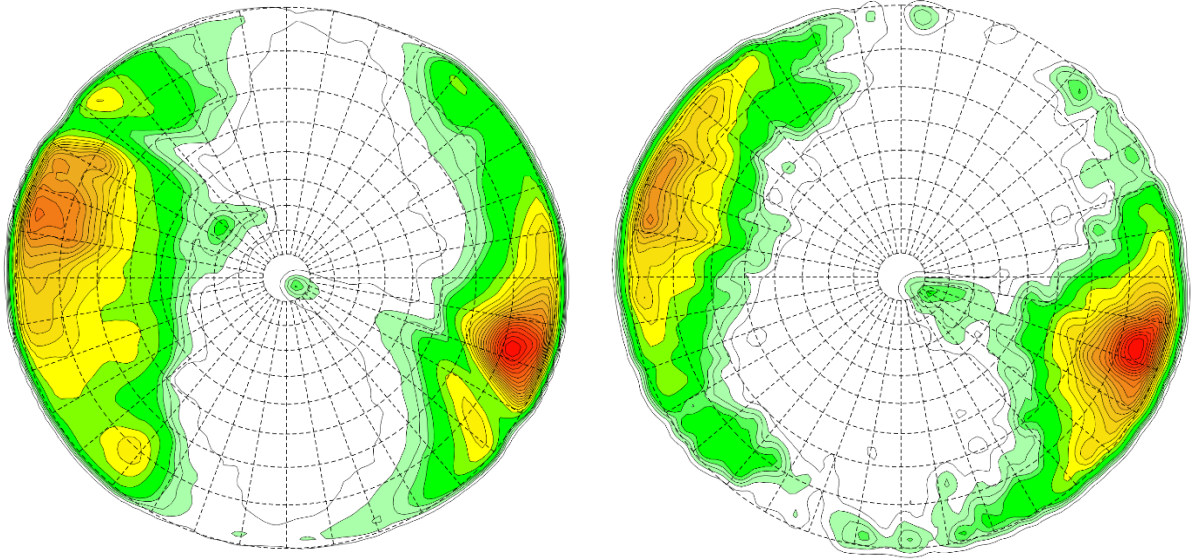


figure 31: The images show Kernel Density Estimations of normal vectors in a stereographic projection for the location Long Chang. High densities are coloured in red. The left image depicts the densities of the normal vectors of every point of the point cloud, whereas the right image displays the densities of normal vectors of all planes, computed during the semi-automatic methodology. The comparison shows slightly higher performance for the depiction of plane normal vectors (right image).

table 7: The average set dip direction/ dip value for all three datasets, for both methodologies are listed. For the semi-automatic methodology, the initial centre estimation, based on the KDE and the final orientations, derived from the clustering analysis are listed.

set	1	2	3	4	5	6
Long Chang (automatic – initial estimation)	045/90	075/90	288/90	155/90	005/90	300/12
Long Chang (automatic – final orientation)	049/87	080/89	291/87	150/89	004/86	299/17
Long Chang (supervised)	039/87	073/88	112/89	144/87	181/89	306/09
Xiang Qi Jiang Kou (automatic – initial estimation)	225/90	75/90	110/90	155/90	190/90	180/25
Xiang Qi Jiang Kou (automatic – final orientation)	220/89	070/89	115/89	154/89	185/89	179/30
Xiang Qi Jiang Kou (supervised)	226/89	080/90	115/89	148/88	186/89	174/19
Lao Hu Po coalmine (automatic – initial estimation)	205/90	235/90	275/90	305/90	355/90	230/25
Lao Hu Po coalmine (automatic – final orientation)	209/88	238/89	270/89	305/89	000/89	232/30
Lao Hu Po coalmine (supervised)	208/89	060/90	089/90	126/90	348/89	239/18

The final mean discontinuity set orientations derived from both methodologies are listed in table 7. The comparison of the results of both methodologies shows maximum differences in the dip direction of  $10^\circ$  for the Long Chang and Xiang Qi Jiang Kou data and  $12^\circ$  for the Lao Hu Po coalmine data. The dip value of the sets 1 to 5, which are all sub-vertical, is nearly the same for both methodologies. Considering the low data resolution and the general difficulties in set orientation determination due to the high variation in discontinuity orientation (section 3.2.), these results are similar. A statement about superior accuracy of any methodology regarding these results cannot be made. The figures 33 to 39 show the similarities of the two models. A slight shift in set orientations between the models can be observed. In table 7 also the initial centre orientations for the clustering algorithm, derived from the KDE during the semi-automatic methodology, are listed. They do not differ more than  $5^\circ$  from the final orientation, as this condition is implemented in the clustering algorithm (section 5.1.2.3.).

The dip value of the sixth set from table 7, which is geologically a bedding plane, is between  $8^\circ$  and  $12^\circ$  higher in the results of the semi-automatic methodology. In figure 32 planes were modelled along the bedding plane traces using the software CloudCompare. With this method the accurate bedding orientation can be determined. Measurements of these modelled planes confirm the results of the supervised methodology. During the supervised methodology the planes, which are modelled for orientation measurements, are assessed geologically by the editor and can be deleted or processed if they do not seem reasonable. In this case the bedding traces, mostly represented by missing points in the point cloud, were observed and supported the modelling of correct bedding planes. This task cannot be performed by the semi-automatic algorithm. Since the bedding planes are rarely visible, but mostly only their traces, only few bedding planes are grown during the semi-automatic methodology and thus only few orientation measurements are made. The weathered, curvy shapes between the sub-horizontal bedding plane and the vertical fracture sets, best visible in figure 37 and 38, shift the bedding orientation to a higher dip value. This results in a noticeable error for the dip value of the bedding set in the results of the semi-automatic methodology. Results obtained by the semi-automatic methodology therefore must always be verified by a geologist before certainty on their accuracy is achieved, especially if discontinuities in the point cloud are mainly represented by traces rather than distinct planes.

The cone of confidence  $\vartheta$  (section 5.1.2.3., formula 31), which is a value for the reliability of the centre orientation, proved to be not presentable, as for big numbers of normal vectors  $\vartheta$  converges to zero. This suggests a high confidence, which is not reached to this extent, as the assignment of the computed planes to the sets is not definitely and only determined by the clustering algorithm.

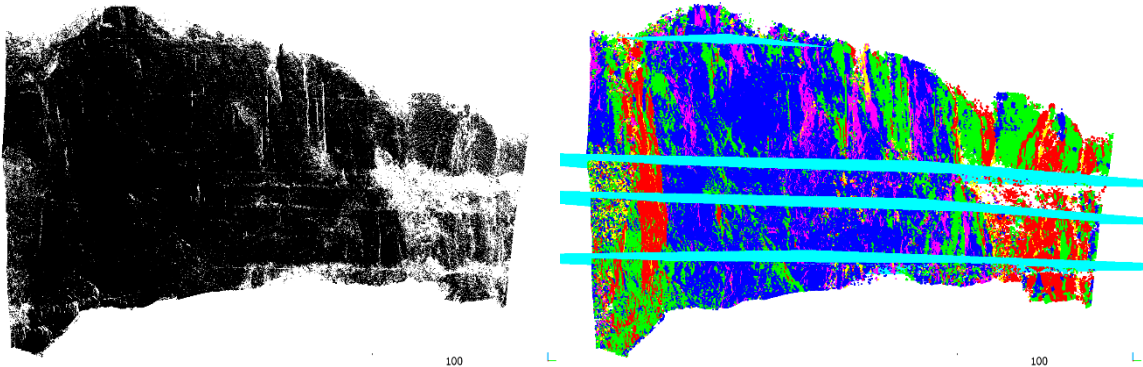


figure 32: In the right image planes were modelled through the horizontal traces of Long Chang, using the software CloudCompare. In the left image the traces are visible as missing points in the raw point cloud. The modelled planes are oriented in the direction  $310/08$  and confirm the result for the bedding obtained by the supervised methodology.

table 8: This table gives a brief overview on the advantages and disadvantages of the discussed methodologies.

Supervised methodology	Semi-automatic methodology
Requires geologist’s working time	For the bigger part automated
Reproducibility is dependent on editor	High reproducibility
Human bias is possible	Hardly influenced on human bias
Noise is removed by manual segmentation	Plane growth removes noise and non-planar structures
Low number of plane measurements, manually with software RiSCAN	High number of plane measurements, fully automated
Planes represented by traces in the rock mass can be considered	Only distinct planes can be measured (not traces)
The result is already verified by the geologist in charge.	The result must be verified!

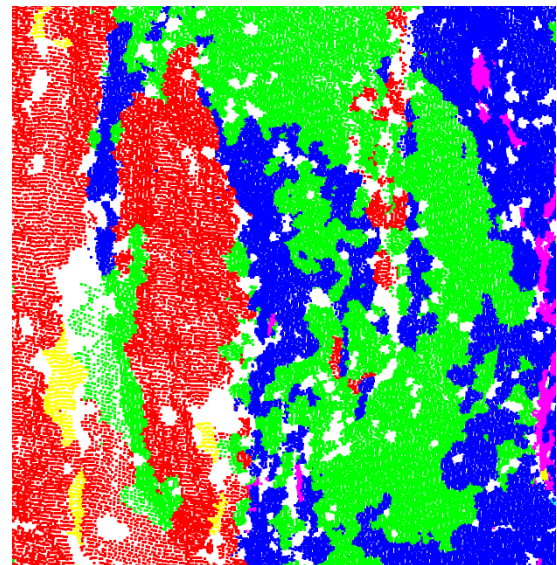
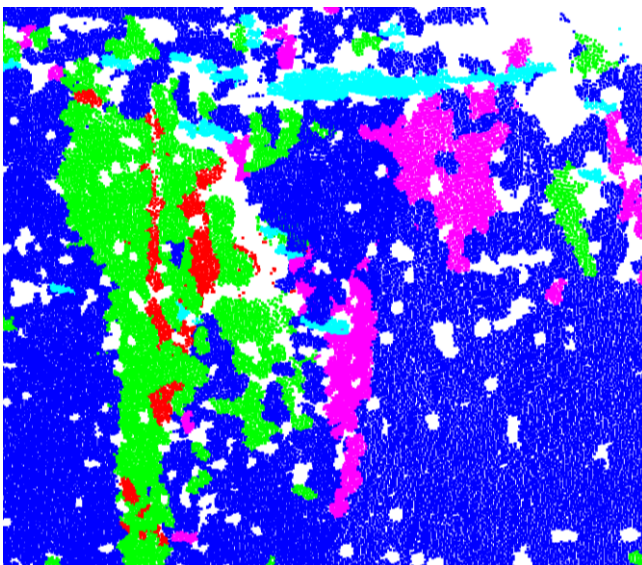
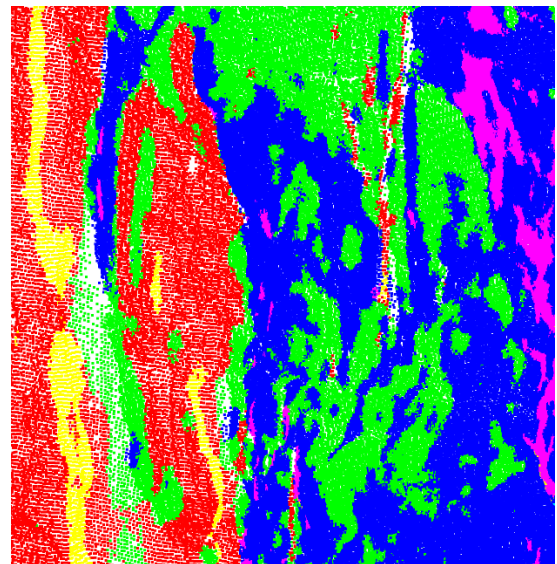
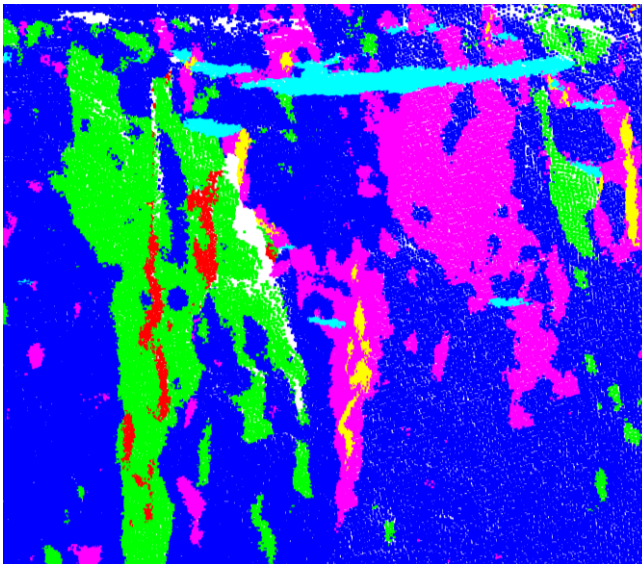
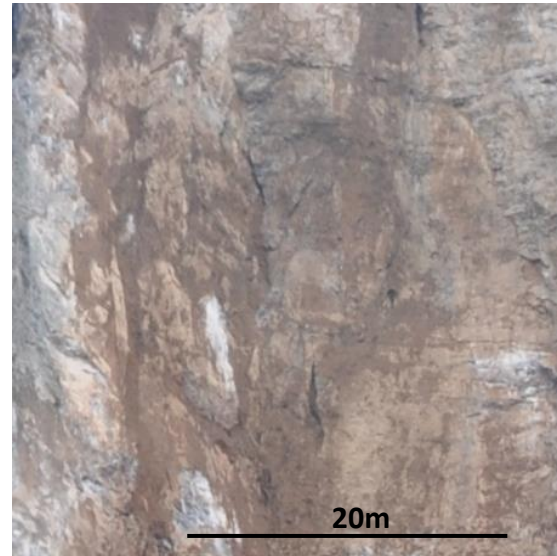
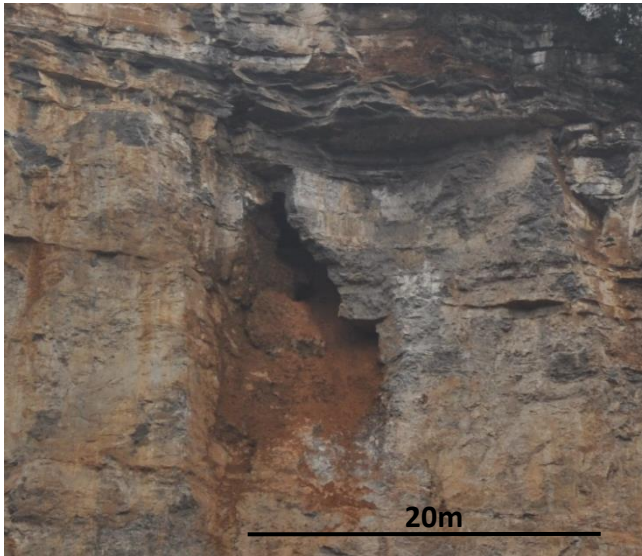


figure 33: The three images show the same detail of the hole, created by karst formation, at Long Chang (depict in figure 2 to 4). (top image: photography, middle image: supervised model, bottom image: semi-automatic model)

figure 34: The images (top: photography, middle: supervised model, bottom: semi-automatic model) show the intersection at Long Chang, which was part of the most recent rock fall.

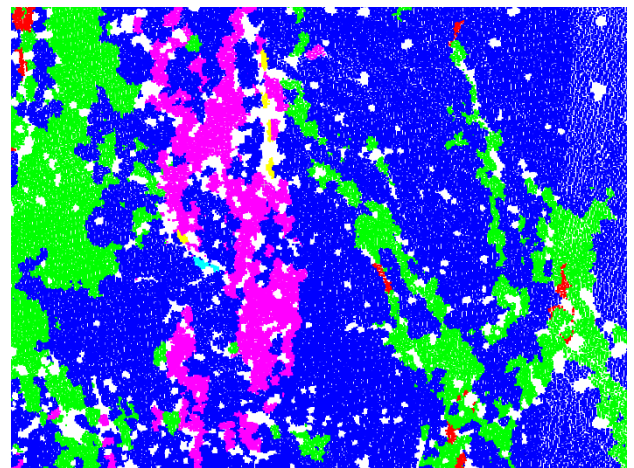
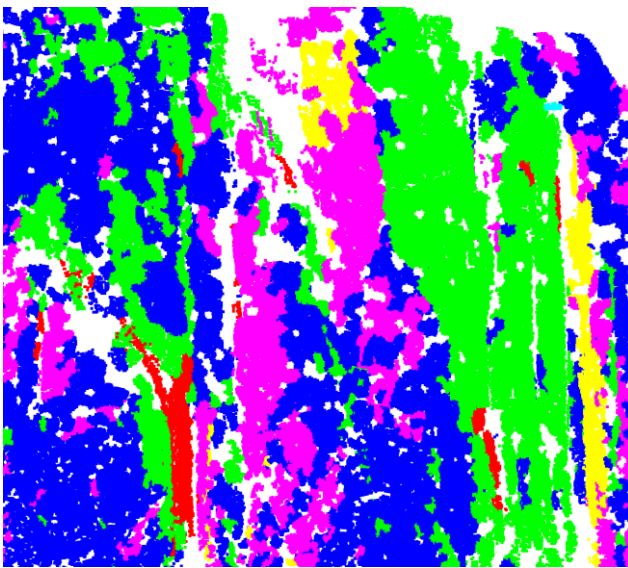
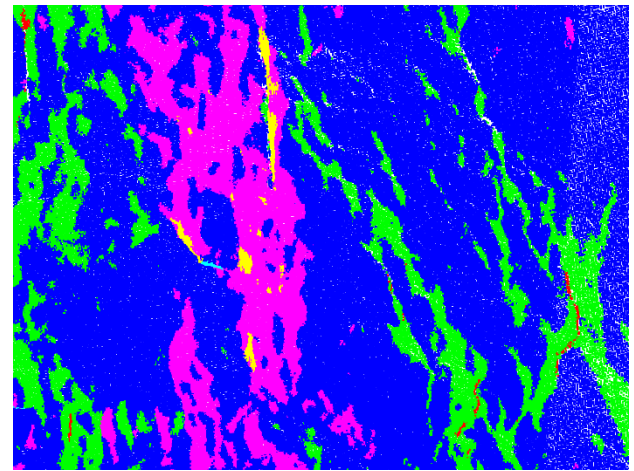
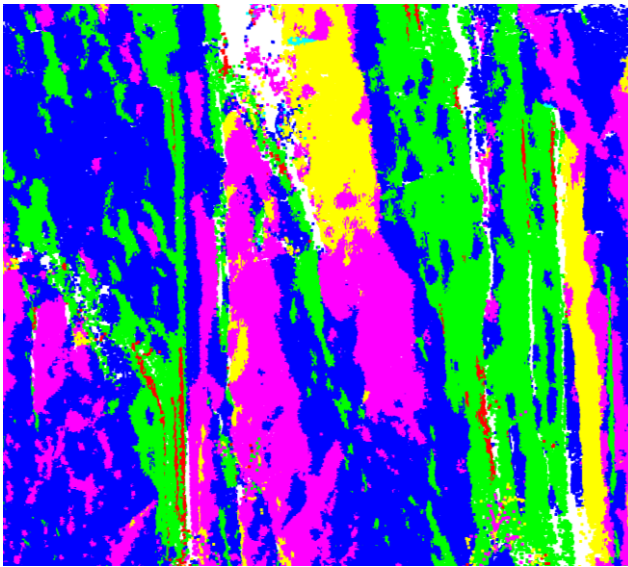
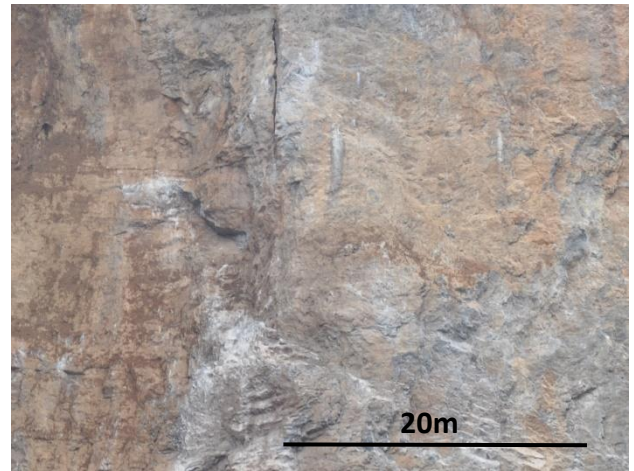
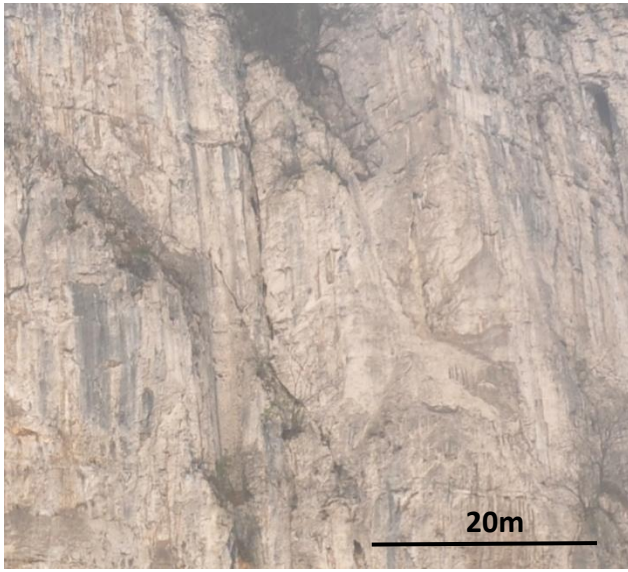


figure 35: The three images (top: photography, middle: supervised model, bottom: semi-automatic model) each show the same detail in the north of the Long Chang outcrop.

figure 36: Three images (top: photography, middle: supervised model, bottom: semi-automatic model) of the same detail, in the centre of the outcrop Long Chang, are displayed for comparison.

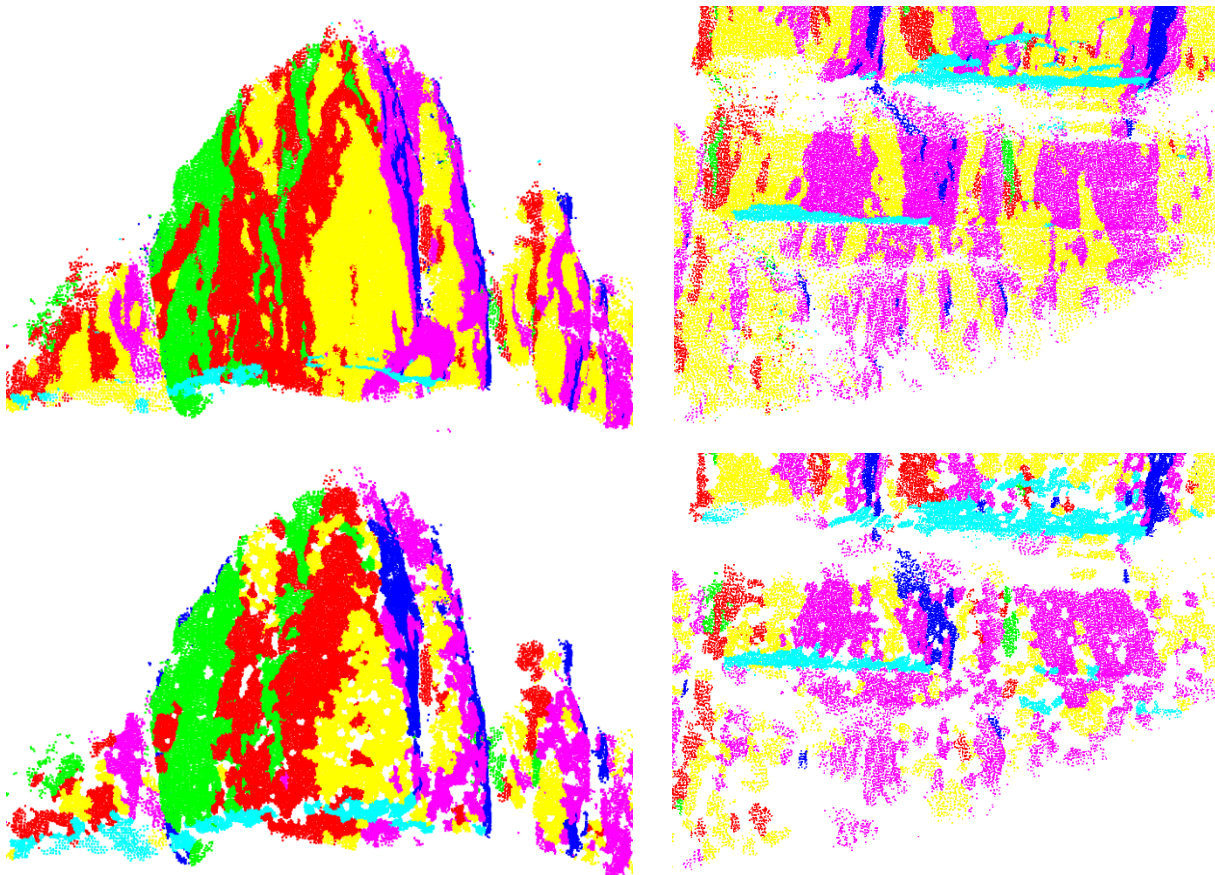
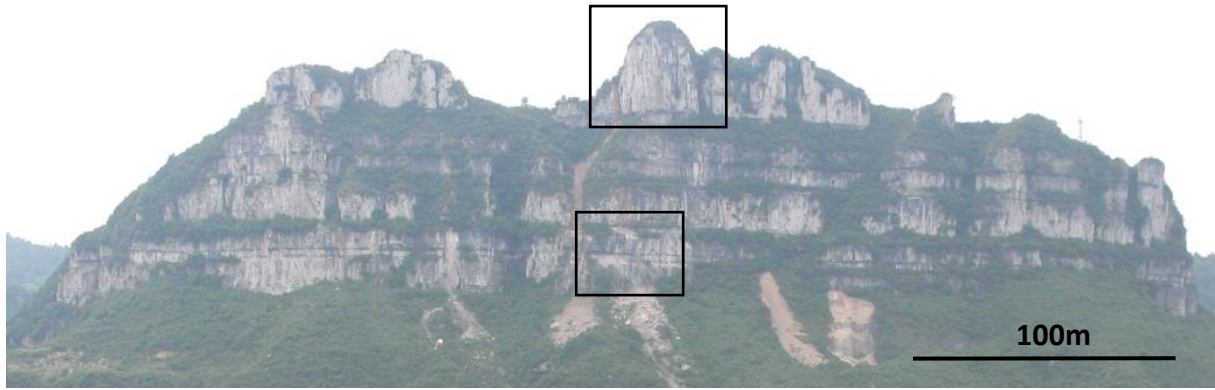


figure 37: In the uppermost photography of the outcrop Xiang Qi Jiang Kou two details are marked by black rectangles. The models of the upper tower-like structure are displayed in the two left images (upper: supervised, lower: semi-automatic). The two models of the lower face are displayed in the right images (upper: supervised, lower: semi-automatic). The models show, even though computed with different methodologies, high similarity. A transition between the horizontal bedding planes (cyan) and the sub vertical fractures can be observed, which is formed by rounded, weathered shapes. Measurements of these planes, during the semi-automatic methodology, led to a dip value for the bedding plane which is too high.

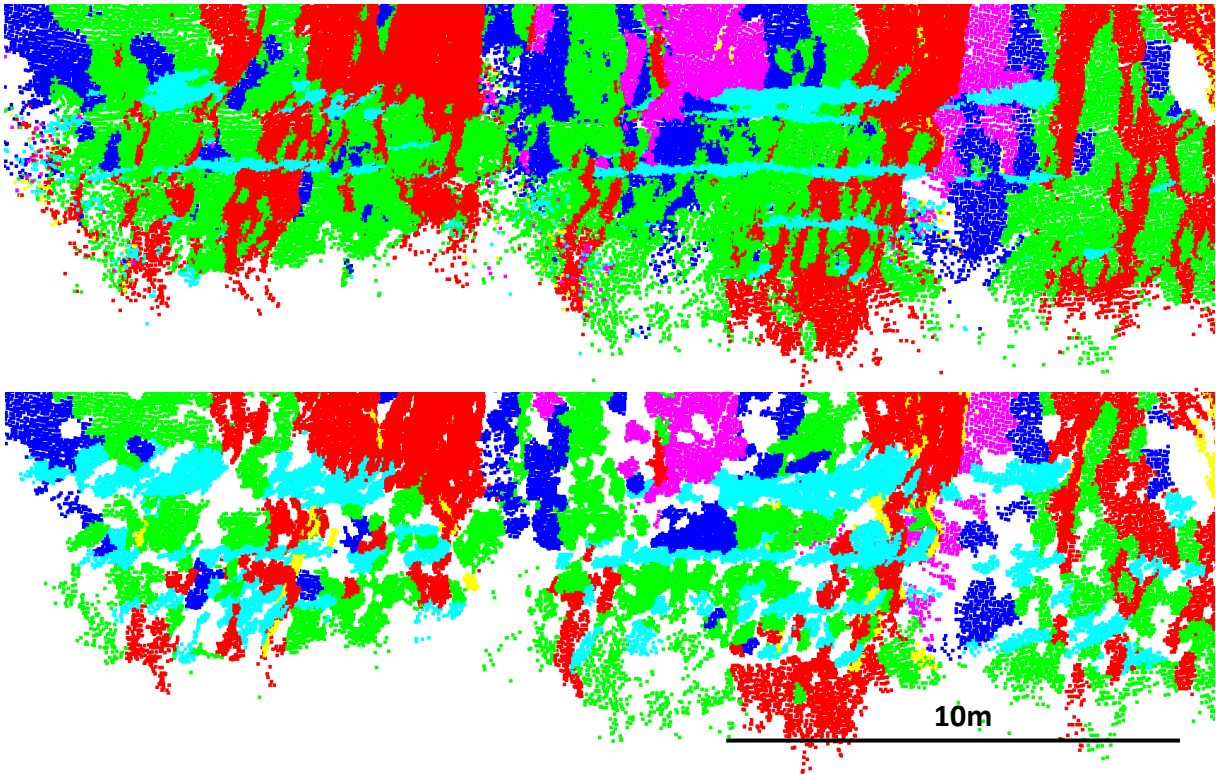


figure 38: The upper image shows a detail of the Lao Hu Po coalmine outcrop from the supervised model. The lower image shows the same detail from the semi-automatic model. Rounded shapes between the relatively horizontal bedding planes (cyan) and the steep fracture planes have formed due to weathering and led to the error of the bedding orientation in the results of the semi-automatic methodology.

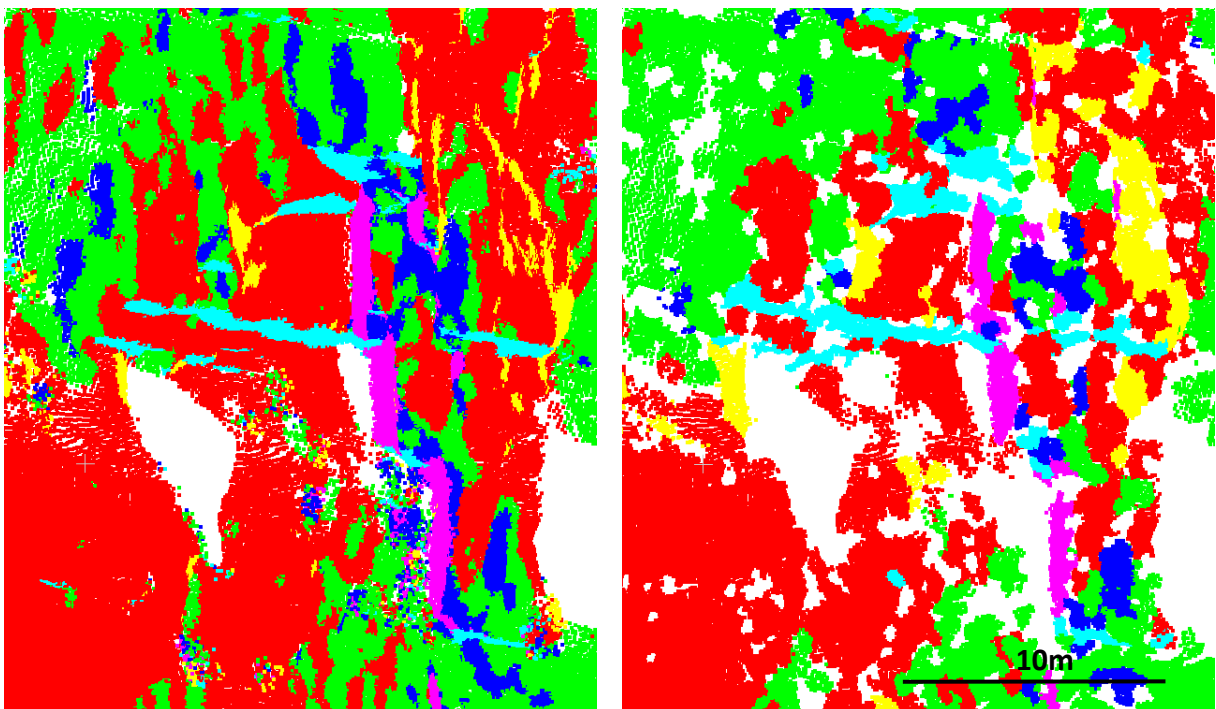


figure 39: The left figure shows a detail in the model created with the supervised methodology at the location Lao Hu Po coalmine. The right image shows the same detail in the semi-automatic model.

## 6. Stability analysis

The correct determination of the discontinuity set orientation is the critical aspect for the stability analysis of a rock mass. The presentation of two methods to obtain this data is the main issue of this thesis, however eventually a statement about the stability regarding different failure modes must be made. By considering the orientations of the discontinuities in relation to the face, it can be stated whether failure is geometrically possible. Though the geometrical disposition, which is analysed here, is necessary, it only describes the possibility of failure, while other discontinuity parameters such as persistence, connectivity, filling, roughness and the existence of rock bridges are not considered. A simple extension to the purely kinematic consideration is made by including the friction angle, which is assumed to be  $30^\circ$ .

### 6.1. Failure Modes

The maintained discontinuity set data is processed by a simple stability analysis, concerning the three failure modes planar sliding, wedge sliding and toppling. These failure modes occur in discontinuous rock where the intact rock strength is significantly higher than the strength of the discontinuities [24].

### 6.1.1. Planar sliding

Planar sliding is a mechanism where a block slides on a single discontinuity plane. For this failure mode two conditions must be fulfilled. First the dip direction of the sliding plane must be sub-parallel to the face dip direction. The maximum allowed deviation from parallelism can be determined by lateral limits, which in this project are set to  $20^\circ$  as suggested by Hudson and Harrison (1997). The second purely kinematic condition requires the discontinuity plane to be less steep than the face, to allow the daylighting of the sliding plane. This criterion is extended for the semi-kinematic consideration. The dip value of the sliding plane must be steeper than the angle of friction, so the driving forces exceed the resisting forces [24].

### 6.1.2. Wedge sliding

For wedge sliding two planes, along which simultaneous sliding occurs, are necessary. The sliding direction is the intersection's trend. The intersection's trend must not deviate more than  $90^\circ$  from the face's dip direction and the dip of the face must exceed the plunge of the intersection, to enable the daylighting of the intersection. The intersection must dip steeper than the friction angle, assuming both planes have the same friction angle. For wedge sliding there are no lateral limits, as there is a further degree of freedom due to the second plane involved. However, intersections with a trend closer to the face's dip direction are more critical [24].

### 6.1.3. Toppling

There are two forms of toppling. Flexural toppling occurs in layered rock, consisting of column shaped blocks, which steeply dip in the direction opposite to the face, causing a slip between the columns and consequent bending. Direct toppling occurs with more compact block forms, when the centre of gravity lies outside the contact plane between the block and the rock mass, leading to the overturning of the block [24]. For this project direct toppling was considered, as the general block form is compact and not column shaped. Direct toppling occurs when two criteria are fulfilled. First a sub vertical intersection of two planes, which dips into the face, exists. Second a release plane, which forms complete blocks, is necessary [24].

## 6.2. Methodology

For the stability analysis of the three failure modes discussed in section 6.1. the face orientation, discontinuity normal vectors and calculated intersections are plotted in a stereographic projection. The data obtained from both methodologies is processed separately. First, the discontinuity set which forms the overall face orientation is determined. The face orientations for all three locations and both methodologies are listed in table 9 (supervised methodology) and 10 (semi-automatic methodology). All measurements of discontinuities assigned to the set which forms the overall face, are excluded from the analysis, as it is assumed that discontinuities of the same set do not intersect. For the data of the supervised methodology, the software Dips is used to carry out the kinematic analysis. The input parameters are the face orientation, the friction angle, and the lateral limits. For the semi-automatic methodology, a simple semi-kinematic analysis is implemented with MATLAB. The computed mean normal vectors and the spherical aperture, to depict the variability in orientation, are displayed. Ten Intersections are calculated from the remaining five mean normal vector orientations, as the set representing the face orientation is excluded. This is achieved by computing the cross product of every normal vector pair. In this plot only the mean intersection orientation is depicted without considering its variability. To display the variability all possible intersections are calculated and plotted in an independent stereographic projection using the Kernel Density Estimation (section 5.1.2.2.).

For planar sliding a critical area for normal vectors, which lies inside the great circle of the plane perpendicular to the face, outside the angle of friction drawn from the centre and inside the lateral limits, is coloured in red. Intersections are critical regarding wedge sliding when they plot in the red area, which is defined outside the great circle of the face and inside the friction angle drawn from the perimeter. Intersections that lie in the yellow area of the stereographic projection computed with Dips, which is the secondary critical zone for wedge sliding, are less steep than the friction angle but sliding can occur, as one of the two planes is steeper than the friction angle. For direct toppling two criteria must be fulfilled. First, intersections plot in the red area, which is defined as the sector inside the plane perpendicular to the face and inside the lateral limits. Second, normal vectors must plot inside the semicircle of the friction cone, drawn from the centre, that lies opposite to the face, to function as release planes. Only if both criteria are fulfilled, direct toppling is geometrically possible.

## 6.3. Results

### 6.3.1. Supervised methodology

The results for the kinematic analysis, computed with the software Dips using the data obtained by the supervised methodology, for all three outcrops Long Chang, Xiang Qi Jiang Kou and Lao Hu Po coalmine are displayed in the figures 40 to 42. Each figure shows the stereographic projections for all three failure modes, at one outcrop. The face orientations used are listed in table 9.

table 9: The face's dip direction and dip value, which are used for the kinematic analysis of the data obtained from the supervised methodology, are listed.

	<b>dip direction</b>	<b>dip value</b>
<b>Long Chang</b>	112	89
<b>Xiang Qi Jiang Kou</b>	006	90
<b>Lao Hu Po coalmine</b>	28	90

At all three locations planar failure is geometrically unlikely as there are rarely discontinuities which daylight the face within the lateral limits of 20°. Only few normal vectors plot in the critical red area. This instance changes if lateral limits are raised or if the face orientation is slightly changed, however generally the risk of planar failure is low. According to this analysis none of the three outcrops is at risk for direct toppling, as only one of two criteria is fulfilled. Steep intersections trending towards the face exist, however there are no release planes dipping in the same direction as the face. At all three locations the bedding plane dips with a small angle towards the face and therefore cannot function as such. Outcrops where the bedding plane dips out of the face have probably existed but have eroded faster, as this constellation is at high risk for direct toppling. Consequently, in this thesis only relatively stable configurations regarding the bedding plane were observed. The problematic failure mode at all investigated locations is wedge sliding. The five subvertical fracture sets form steep intersections trending in all directions. Intersections that daylight the face, which means in the stereographic projection they plot outside the great circle of the face and inside the friction angle drawn from the perimeter, are critical. The critical blocks consist of one or more sub-vertical fractures and a bedding plane on the top-side, which is necessary to form complete blocks.

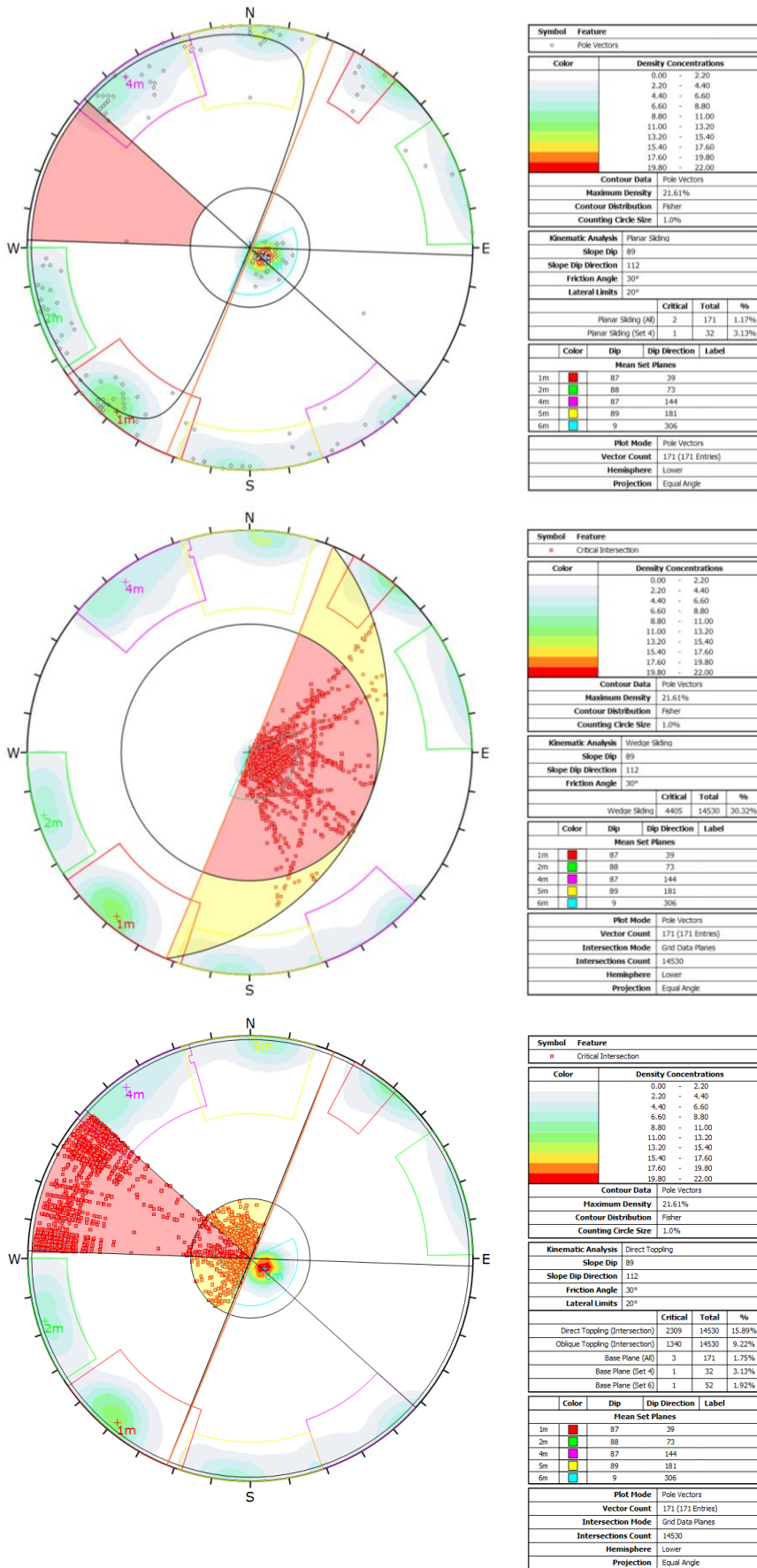
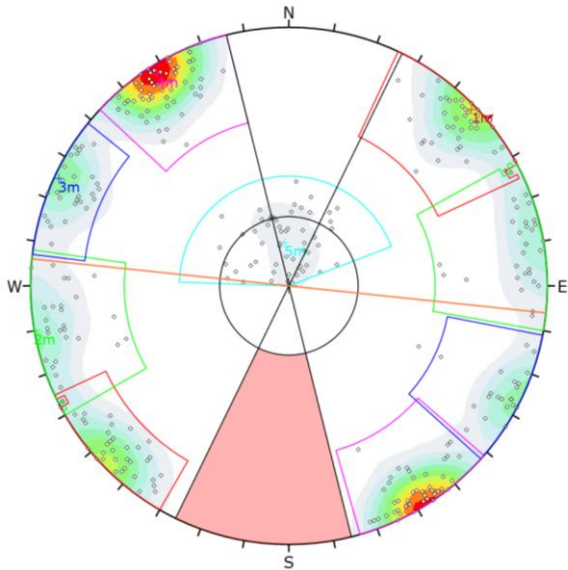


figure 40: The three stereographic projections show the risk of planar failure (topmost image), wedge failure (middle image) and direct toppling (lowermost image) for Long Chang.



Symbol	Feature
○	Pole Vectors

Color	Density Concentrations
0.00	- 1.60
1.60	- 3.20
3.20	- 4.80
4.80	- 6.40
6.40	- 8.00
8.00	- 9.60
9.60	- 11.20
11.20	- 12.80
12.80	- 14.40
14.40	- 16.00

Contour Data	
Maximum Density	15.70%
Contour Distribution	Fisher
Counting Circle Size	1.0%

Kinematic Analysis	
Planar Sliding	
Slope Dip	90
Slope Dip Direction	6
Friction Angle	30°
Lateral Limits	20°

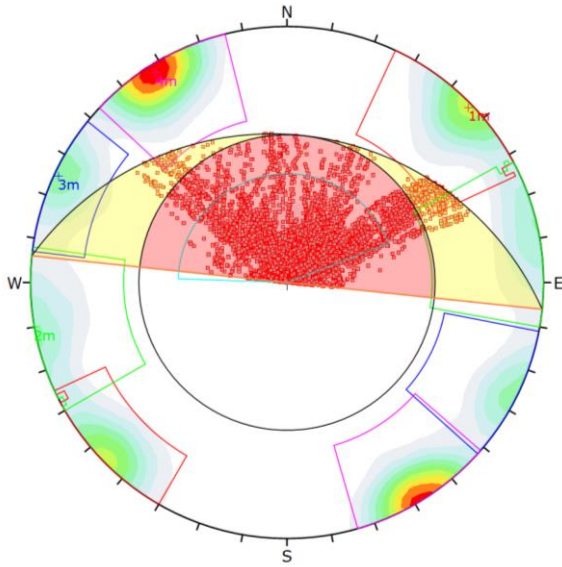
	Critical	Total	%
Planar Sliding (All)	0	346	0.00%

Color	Dip	Dip Direction	Label
1m	89	226	
2m	90	80	
3m	89	115	
4m	88	148	
5m	19	174	

Plot Mode	
Vector Count	346 (346 Entries)
Hemisphere	Lower
Projection	Equal Angle



Symbol	Feature
■	Critical Intersection

Color	Density Concentrations
0.00	- 1.60
1.60	- 3.20
3.20	- 4.80
4.80	- 6.40
6.40	- 8.00
8.00	- 9.60
9.60	- 11.20
11.20	- 12.80
12.80	- 14.40
14.40	- 16.00

Contour Data	
Maximum Density	15.70%
Contour Distribution	Fisher
Counting Circle Size	1.0%

Kinematic Analysis	
Wedge Sliding	
Slope Dip	90
Slope Dip Direction	6
Friction Angle	30°

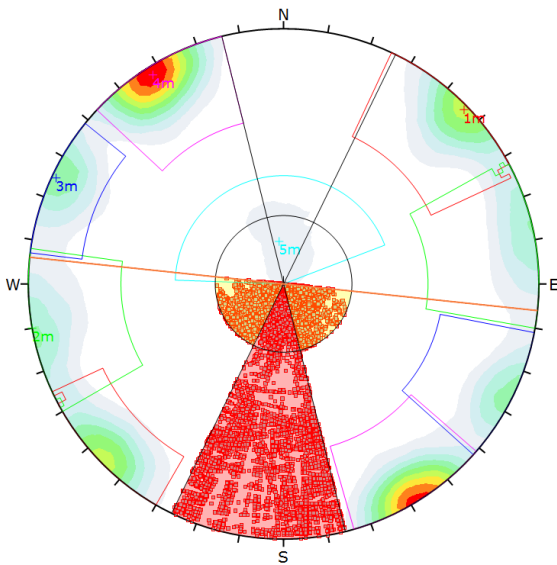
	Critical	Total	%
Wedge Sliding	18181	59672	30.47%

Color	Dip	Dip Direction	Label
1m	89	226	
2m	90	80	
3m	89	115	
4m	88	148	
5m	19	174	

Plot Mode	
Vector Count	346 (346 Entries)
Intersection Mode	Grid Data Planes
Intersections Count	59672
Hemisphere	Lower
Projection	Equal Angle



Symbol	Feature
■	Critical Intersection

Color	Density Concentrations
0.00	- 1.60
1.60	- 3.20
3.20	- 4.80
4.80	- 6.40
6.40	- 8.00
8.00	- 9.60
9.60	- 11.20
11.20	- 12.80
12.80	- 14.40
14.40	- 16.00

Contour Data	
Maximum Density	15.70%
Contour Distribution	Fisher
Counting Circle Size	1.0%

Kinematic Analysis	
Direct Toppling	
Slope Dip	90
Slope Dip Direction	6
Friction Angle	30°
Lateral Limits	20°

	Critical	Total	%
Direct Toppling (Intersection)	9125	59672	15.29%
Oblique Toppling (Intersection)	13159	59672	22.05%
Base Plane (All)	1	346	0.29%
Base Plane (Set 5)	1	56	1.79%

Color	Dip	Dip Direction	Label
1m	89	226	
2m	90	80	
3m	89	115	
4m	88	148	
5m	19	174	

Plot Mode	
Vector Count	346 (346 Entries)
Intersection Mode	Grid Data Planes
Intersections Count	59672
Hemisphere	Lower
Projection	Equal Angle

figure 41: The risk of planar failure (topmost image), wedge failure (middle image) and direct toppling (lowermost image) for Xiang Qi Jiang Kou is depicted in the three projections.

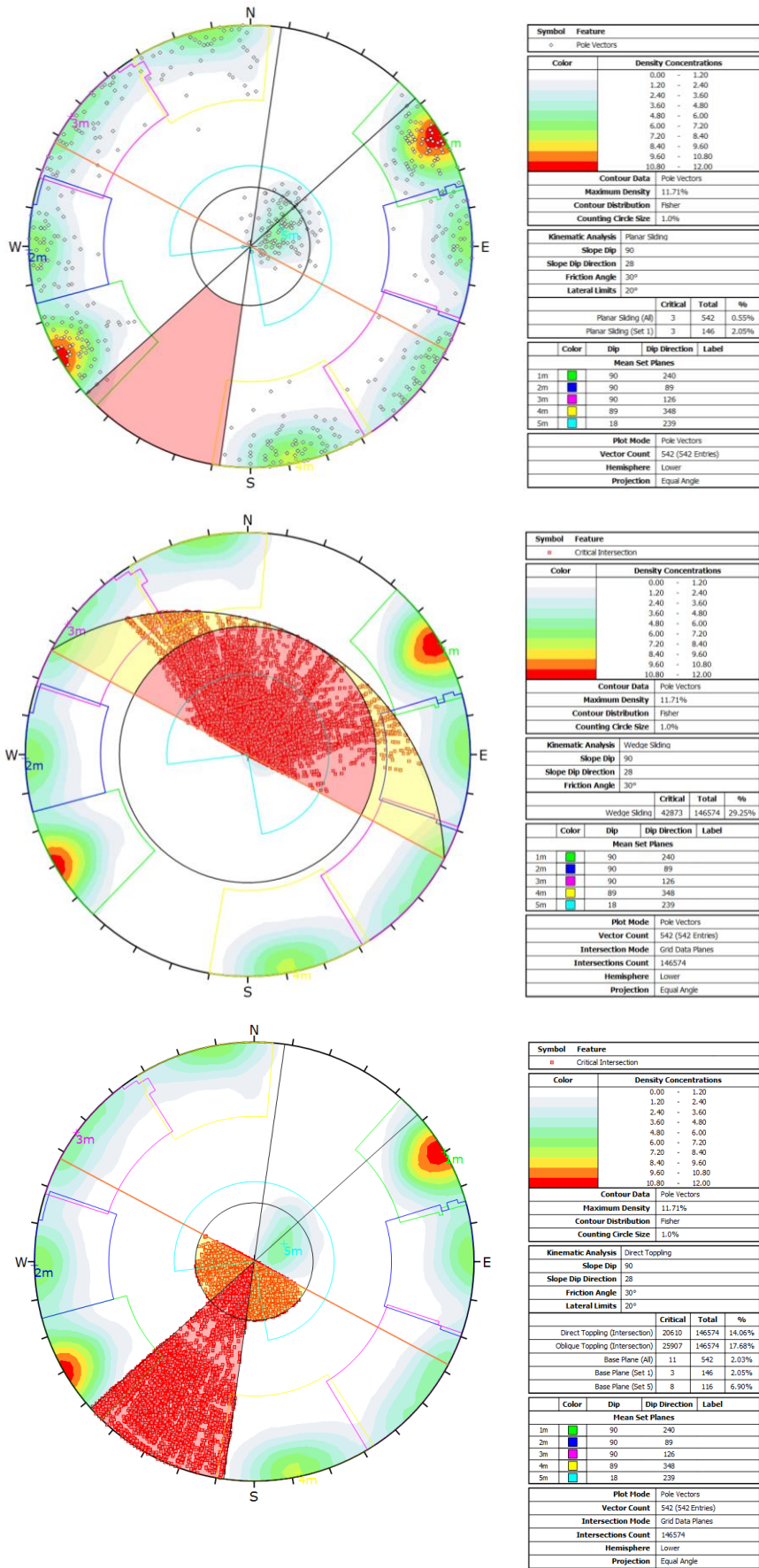


figure 42: The three stereographic projections show the risk of planar failure (topmost image), wedge failure (middle image) and direct toppling (lowermost image) for Lao Hu Po coalmine.

### 6.3.2. Semi-automatic methodology

The results of the kinematic analysis for the semi-automatically derived data, computed with MATLAB, are depicted in the figures 43 to 45 for all three locations Long Chang, Xiang Qi Jiang Kou and Lao Hu Po coalmine. Each image depicts the risk of all three discussed failure modes at one location. For wedge failure at all three locations a further stereographic projection is depicted in figure 46, where all computed intersections are displayed using the Kernel Density Estimation, to show the variability in the intersections' orientation. The used face orientations are listed in table 10.

table 10: This table lists the face orientations of the three outcrops used for the stability analysis of the semi-automatic methodology.

	<b>dip direction</b>	<b>dip value</b>
<b>Long Chang</b>	111	90
<b>Xiang Qi Jiang Kou</b>	005	90
<b>Lao Hu Po coalmine</b>	029	90

As the orientations derived from both methodologies are similar, the kinematic analysis delivered the same results as well. The risk of planar failure for all three outcrops is low as only the edges of the spherical apertures intersect the critical, red area of the stereographic projection. Direct toppling is also not classified as a critical failure mechanism at all three locations for this analysis. Even though intersections plot in the critical, red area, there are not any normal vectors, which plot in the yellow area of the stereographic projection, to function as release planes. Wedge sliding is the only critical failure mode for all three locations, as the steeply dipping discontinuity sets form steep intersections. It must be considered that even if intersections plot outside the critical, red area of the figures 43 to 45, the variability in the intersections' orientation is not displayed in these projections. Consequently, intersections just outside the red area are critical indeed. In figure 46, where the densities of all intersections are displayed, this variability becomes visible. High densities are observed in the critical area. The intersections are calculated by computing all possible cross products between the normal vectors of every pair of sets. Intersections where the bedding plane is involved are hardly represented in this plot, because their densities are low, as only few bedding planes were computed during the plane growing process.

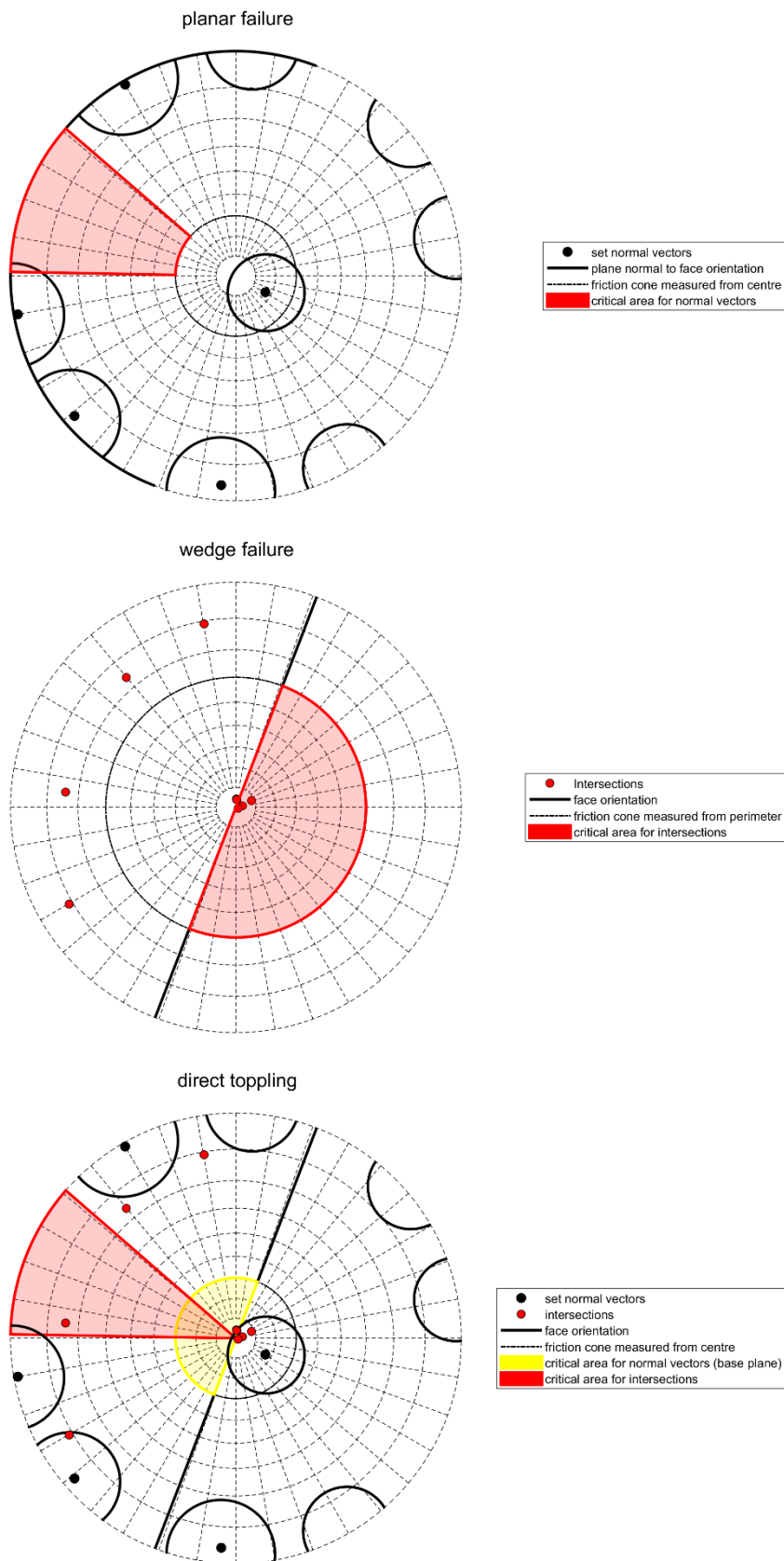


figure 43: The three images show the risk of planar sliding (uppermost), wedge sliding (middle) and direct toppling (lowermost) for the data obtained by the semi-automatic methodology for the location Long Chang.

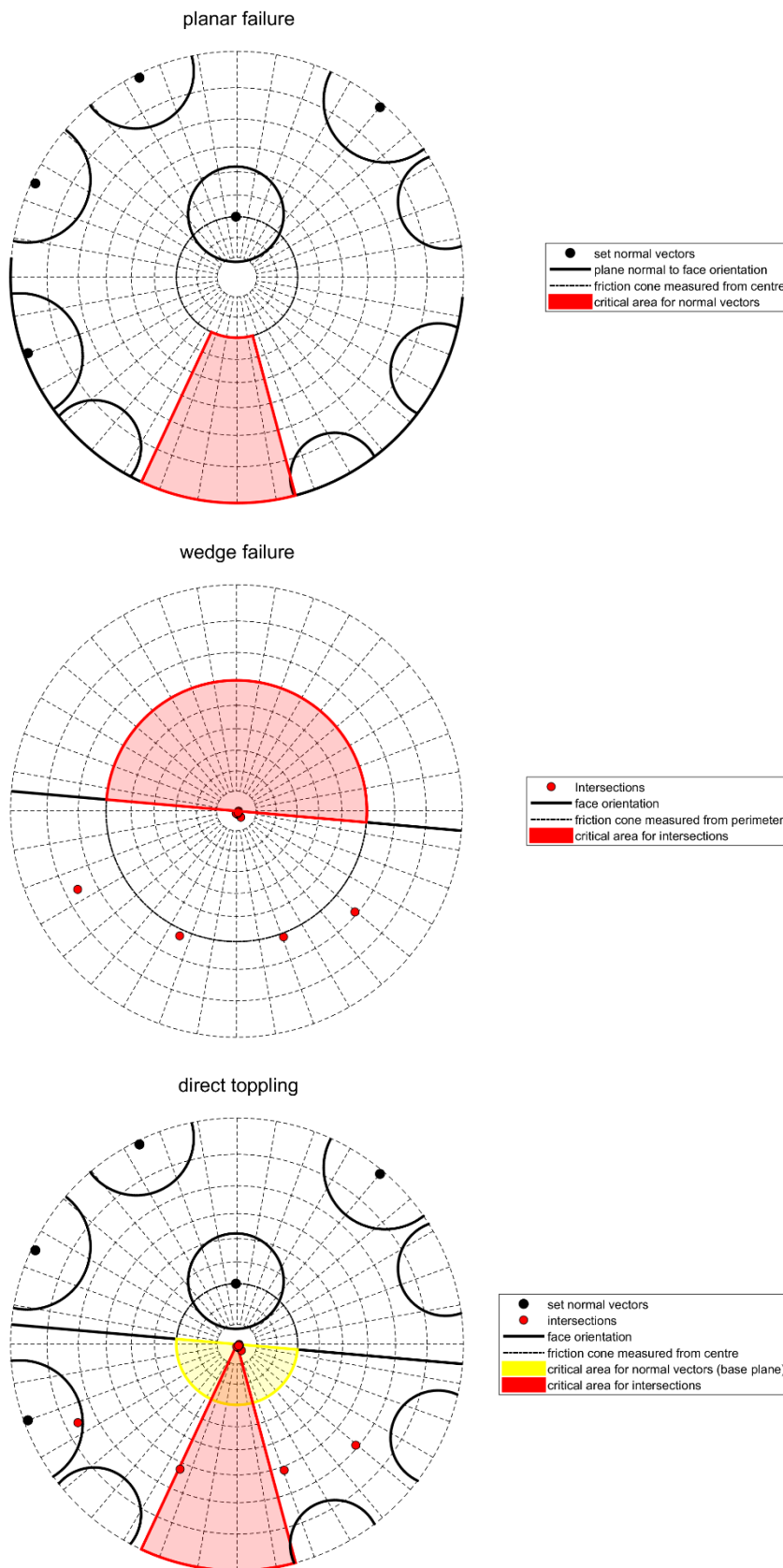


figure 44: The risk of planar sliding (uppermost), wedge sliding (middle) and direct toppling (lowermost) at the location Xiang Qi Jiang Kou is determined, using the data of the semi-automatic methodology.

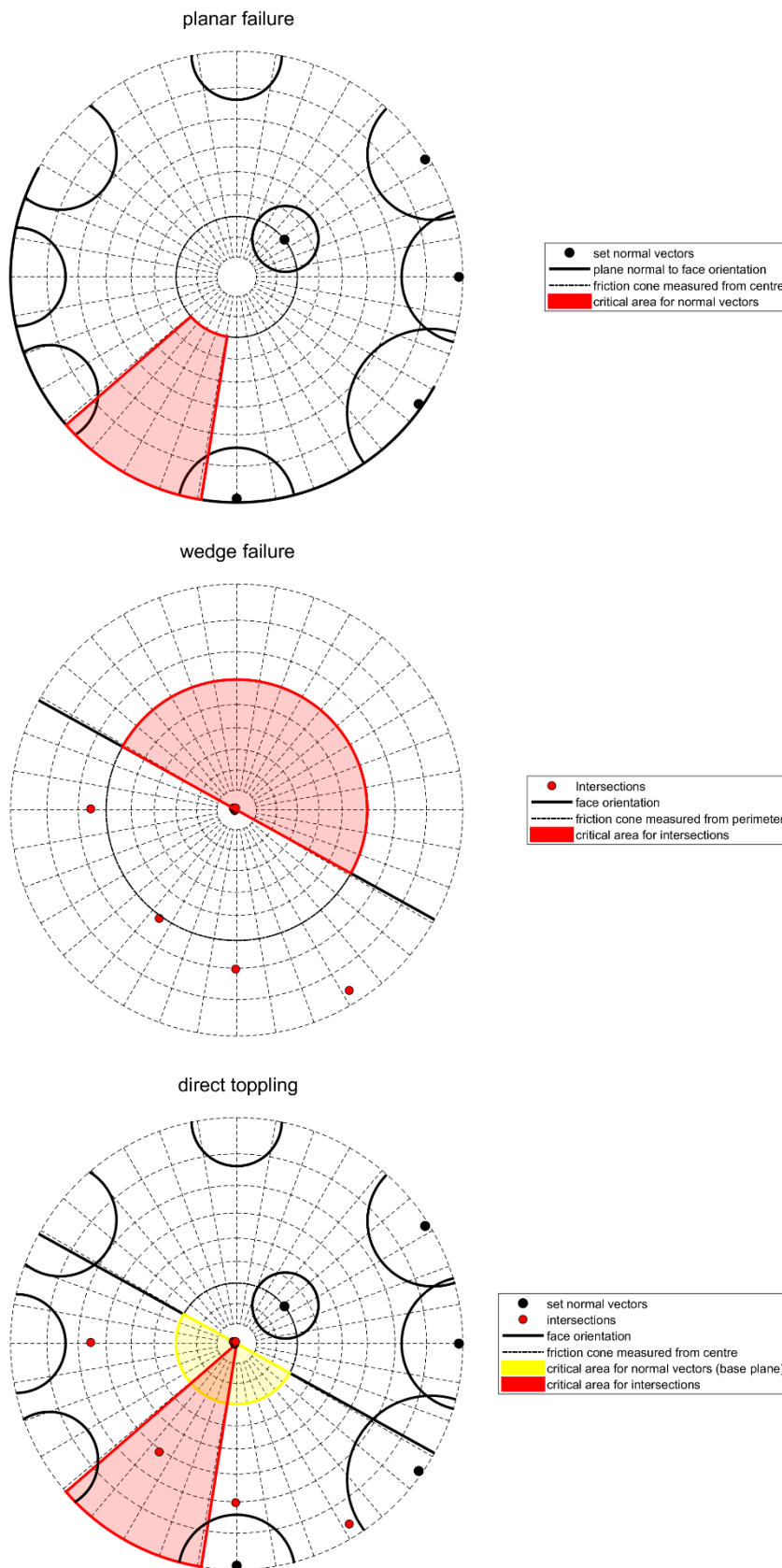


figure 45: The three images show the risk of planar sliding (uppermost), wedge sliding (middle) and direct toppling (lowermost) for the data obtained by the semi-automatic methodology for the location Lao Hu Po coalmine.

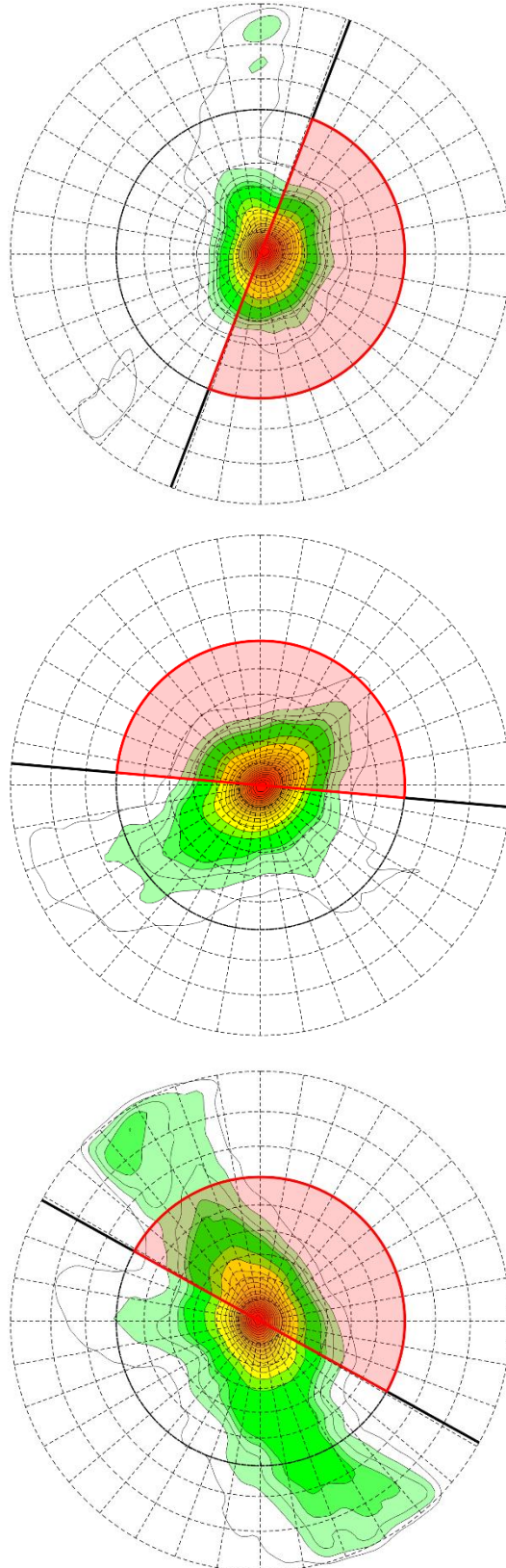


figure 46: All possible intersections of planes, grown during the semi-automatic methodology, are calculated and depict in the stereographic projection using the KDE. The red surface represents the critical area for intersections, which are at risk for wedge sliding. The uppermost image depicts the risk of wedge sliding for Long Chang, the middle image for Xiang Qi Jiang Kou and the lowermost image for Lao Hu Po coalmine. Densities increase from green to red.

## 7. Conclusion

The comparison of the two methodologies showed that a semi-automatic methodology can be superior to a supervised methodology in terms of human working time, data quantity and reproducibility. If there are no discontinuities, which are mainly represented by traces in the face, the data quality of the supervised method can also be reached. A geologist's judgement and control, however, is still necessary if the measuring of planes, represented by the points of the point cloud, is not enough to derive the correct orientations of all discontinuity sets. The plane growing algorithm proved to be a beneficial tool to automatically receive a great number of real plane measurements. It is superior to the use of normal vector orientations of all points, as discontinuity sets perpendicular to the face can be identified more reliable and noise and non-planar structures are removed more efficiently. The depiction of big normal vector data in a stereographic projection by using a Kernel Density Estimation, proved to deliver good results.

Generally, three qualifications must be fulfilled to enable the delivery of correct discontinuity set orientations by the semi-automatic methodology. Firstly, the point cloud resolution must be high enough to avoid a resolution bias (section 3.2). Secondly, all discontinuity sets are mainly represented by distinct planes in the face, rather than by traces. This condition is necessary as the plane growing algorithm (section 5.1.2.1.) can only grow and measure planes, which are formed by points of the point cloud. Thirdly, clear discontinuity sets exist in the rock mass and their variances in orientation are moderate. This criterion must be complied to receive clear density peaks in the Kernel Density Estimation (section 5.1.2.2.), which serve as initial centres for the clustering analysis and to justify the assignment of individual plane measurements to certain discontinuity sets. A simplification of the discontinuity orientations of a rock mass to a mean orientation and spherical aperture of discontinuity sets is, for any methodology, only reasonable for clear sets with moderate variances.

The advantages and disadvantages of the semi-automatic methodology need to be confirmed and further investigated by applications on different data sets.

The discontinuity analysis showed six discontinuity sets. Five fracture sets, which dip sub-vertical were detected at all three locations. The bedding, which at all locations dips slightly into the face, changes the dip direction across the field. It is assumed that faces with bedding planes dipping out of the rock mass have eroded fast, as direct toppling is highly critical for this constellation of discontinuities. The extrapolation of the received orientation data to adjacent outcrops is reasonable if the orientation of the bedding plane is considered discretely.

Regarding the rock mass stability, wedge failure turned out to be the critical failure mode. Blocks are formed by one or more intersections of sub-vertical fractures and are completed on their top side by sub-horizontal bedding planes. Planar sliding is not critical, as there are no discontinuities striking sub-parallel to the face, except for the bedding plane, which however dips into the rock mass. Direct toppling is not critical as release planes are missing.

## Reference list

- [1] R.E. Goodman (1989), *Introduction to Rock Mechanics* - 2nd edition, Wiley and Sons, New York
- [2] M. Mohebbi, A.R. Yarahmadi Bafghi, M. Fatehi Marji, J. Gholamnejad (2015), Rock mass structural data analysis using image processing techniques, *Journal of Mining & Environment*, Vol.8, No.1, pp. 61-74
- [3] A. Buyer, W. Schubert (2016), Extraction of discontinuity orientations in point clouds, Conference paper, August 2016
- [4] J. Guo, S. Liu, P. Zhang, L. Wu, W. Zhou, Y. Yu (2017), Towards semi-automatic rock mass discontinuity orientation and set analysis from 3D point clouds, *Computers & Geosciences*, Vol. 103, Issue C, pp. 164–172
- [5] S. Slob, H.R.G.K. Hack, Q. Feng, K. Röshoff, A.K. Turner (2007), Fracture mapping using 3D laser scanning techniques, Conference paper, July 2007
- [6] S. Slob, H.R.G.K. Hack, B. van Knapen, K. Turner, J. Kemeny (2005), A method for automated discontinuity analysis of rock slopes with three-dimensional laser scanning, *Transportation Research Record: Journal of the Transportation Research Board*, Vol. 1913, pp. 187-194.
- [7] M. Vöge, M.J. Lato, M.S. Diederichs (2013), Automated rockmass discontinuity mapping from 3-dimensional surface data, *Engineering Geology*, Vol. 164, pp. 155–162
- [8] E. Grilli, F. Menna, F. Remondino (2017), A review of point cloud segmentation and classification algorithms, *The International Archives of the Photogrammetry Remote Sensing and Spatial Information Sciences*, Volume XLII-2/W3
- [9] M. Jaboyedoff, R. Metzger, T. Oppikofer (2007), New insight techniques to analyze rock-slope relief using DEM and 3D imaging cloud points: COLTOP-3D software, *Rock mechanics: Meeting Society's Challenges and Demands*, Vol. 1, pp. 61-68.
- [10] A.J. Riquelme, A. Abellán, R. Tomás, M. Jaboyedoff (2014), A new approach for semi-automatic rock mass joints recognition from 3D point clouds, *Computers & Geosciences*, Vol. 68, pp. 38–52
- [11] G. Gigli, N. Casagli (2011), Semi-automatic extraction of rock mass structural data from high resolution lidar point clouds, *International Journal of Rock Mechanics and Mining Sciences*, Vol. 48, pp. 187–198
- [12] M.J. Lato, M.S. Diederichs, D.J. Hutchinson (2010), Bias Correction for View-limited Lidar Scanning of Rock Outcrops for Structural Characterization, *Rock Mechanics and Rock Engineering*, Vol. 43, pp. 615–628
- [13] R.D. Terzaghi (1965), Source of error in joint surveys. *Geotechnique*, Vol. 15, pp. 287-304

- [14] M. Sturzenegger and D. Stead (2008), Quantifying discontinuity orientation and persistence on high mountain rock slopes and large landslides using terrestrial remote sensing techniques, *Natural Hazards and Earth System Sciences*, Vol. 9, pp. 267–287
- [15] M. Sturzenegger, D. Stead (2009), Close-range terrestrial digital photogrammetry and terrestrial laser scanning for discontinuity characterization on rock cuts, *Engineering Geology*, Vol. 106, pp. 163–182
- [16] P.V.C. Hough (1962), Method and Means for Recognizing Complex Patterns, US Patent 3069654.
- [17] D. Borrmann, J. Elseberg, K. Lingemann, A. Nüchter (2011), The 3D Hough Transform for Plane Detection in Point Clouds: A Review and a new Accumulator Design, *3D Res.* 02:02003
- [18] K. Esbensen, P. Geladi (1987), Principal Component Analysis, *Chemometrics and Intelligent Laboratory Systems*, Vol. 2, pp. 37-52
- [19] [www.mathworks.com](http://www.mathworks.com)
- [20] J.S. Simono (1996), *Smoothing Methods in Statistics*, Springer-Verlag, New York
- [21] K. Hornik, I. Feinerer, M. Kober, C. Buchta (2012), Spherical k-Means Clustering, *Journal of Statistical Software*, Vol. 50, Issue 10
- [22] E. Wallbrecher (1986), *Tektonische und Gefügeanalytische Arbeitsweisen*, Ferdinand Enke Verlag, Stuttgart
- [23] S.D. Priest (1993) *Discontinuity analysis for rock engineering*, Chapman & Hall, London
- [24] J.A. Hudson, J.B. Harrison (1997) *Engineering rock mechanics – An introduction to the principles*, Elsevier Science Ltd